HHS Public Access

Author manuscript

Sci Immunol. Author manuscript; available in PMC 2019 October 26.

Published in final edited form as:

Sci Immunol. 2019 April 26; 4(34): . doi:10.1126/sciimmunol.aau7523.

TET enzymes augment activation-induced deaminase (AID) expression via 5-hydroxymethylcytosine modifications at the *Aicda* superenhancer

Chan-Wang J. Lio[1,*,†], **Vipul Shukla**[1,†], **Daniela Samaniego-Castruita**[1,‡], **Edahi González-Avalos**[1,‡], **Abhijit Chakraborty**[2], **Xiaojing Yue**[1], **David G. Schatz**[3], **Ferhat Ay**[2], and **Anjana Rao**[1,4,5,6,*]

[1]Division of Signaling and Gene Expression, La Jolla Institute, San Diego, CA, USA.

[2]Division of Vaccine Discovery, La Jolla Institute, San Diego, CA, USA.

[3]Department of Immunobiology, Yale University School of Medicine, New Haven, CT, USA.

[4]Sanford Consortium for Regenerative Medicine, San Diego, CA, USA.

[5]Department of Pharmacology, University of California, San Diego, San Diego, CA, USA.

[6]Moores Cancer Center, University of California, San Diego, San Diego, CA, USA.

Abstract

TET enzymes are dioxygenases that promote DNA demethylation by oxidizing the methyl group of 5-methylcytosine to 5-hydroxymethylcytosine (5hmC). Here, we report a close correspondence between 5hmC-marked regions, chromatin accessibility and enhancer activity in B cells, and a strong enrichment for consensus binding motifs for basic region-leucine zipper (bZIP) transcription factors at TET-responsive genomic regions. Functionally, Tet2 and Tet3 regulate class switch recombination (CSR) in murine B cells by enhancing expression of *Aicda*, which encodes the activation-induced cytidine deaminase (AID) enzyme essential for CSR. TET enzymes deposit 5hmC, facilitate DNA demethylation, and maintain chromatin accessibility at two TET-responsive

*Corresponding author. arao@lji.org (A.R.); lio@lji.org (C.-W.J.L.).
†These authors contributed equally to this work.
‡These authors contributed equally to this work.

Author contributions: C.-W.J.L. and V.S. conceptualized experiments, acquired and analyzed the data, and performed statistical analyses for in vitro and in vivo experiments. D.S.-C. and E.G.-A. performed the majority of the bioinformatics and related statistical analyses (ATAC-seq, CMS-IP, enhancer analysis, WGBS, oxBS-seq, and ChIP-seq) and proofread the manuscript. A.C. performed the expression clustering analysis (TC-seq) and advised on RNA-seq analysis. C.-W.J.L. performed initial bioinformatics analyses, motif analysis, and data visualization. X.Y. provided key reagents and assistance for oxBS-seq experiments. F.A. supervised the bioinformatics analysis and reviewed the manuscript. D.G.S. provided advice and key reagents, interpreted data, and reviewed the manuscript. A.R. supervised and interpreted the data. C.-W.J.L., V.S., and A.R. wrote the manuscript.

SUPPLEMENTARY MATERIALS

immunology.sciencemag.org/cgi/content/full/4/34/eaau7523/DC1

Competing interests: A.R. is a member of the Scientific Advisory Board of Cambridge Epigenetix. The other authors declare no competing financial interests.

Data and materials availability: Data for CMS-IP, ChIP-seq, ATAC-seq, RNA-seq, and oxBS-seq have been deposited to the National Center for Biotechnology Information Gene Expression Omnibus (accession number GSE116208). All (other) data needed to evaluate the conclusions in the paper are present in the paper or the Supplementary Materials.

enhancer elements, *TetE1* and *TetE2*, located within a superenhancer in the *Aicda* locus. Our data identify the bZIP transcription factor, ATF-like (BATF) as a key transcription factor involved in TET-dependent *Aicda* expression. 5hmC is not deposited at *TetE1* in activated *Batf*-deficient B cells, indicating that BATF facilitates TET recruitment to this *Aicda* enhancer. Our study emphasizes the importance of TET enzymes for bolstering AID expression and highlights 5hmC as an epigenetic mark that captures enhancer dynamics during cell activation.

INTRODUCTION

The three TET proteins (ten-eleven-translocation; TET1, TET2, and TET3) are Fe(II)- and α-ketoglutarate–dependent dioxygenases that catalyze the stepwise oxidation of 5-methylcytosine (5mC) to 5-hydroxymethylcytosine (5hmC), 5-formylcytosine (5fC), and 5-carboxylcytosine (5caC) (1, 2). Together, these oxidized methylcytosine (oxi-mC) bases are intermediates in DNA demethylation and may also function as stable epigenetic marks. 5hmC, the most stable and abundant product of TET enzymatic activity, is highly enriched at the most active enhancers and in the gene bodies of the most highly expressed genes, and its presence at enhancers correlates with chromatin accessibility (2, 3). TET proteins regulate several fundamental biological processes, including lineage commitment, and play important roles in embryonic, neuronal, and hematopoietic development (3).

TET proteins, particularly TET2 and TET3, have critical roles in B cell differentiation and malignancy (2). We and others have previously shown that deletion of *Tet2* and *Tet3* at early stages of mouse B cell development with an *Mb1-Cre* transgene resulted in impaired light-chain rearrangement and developmental blockade, leading to acute precursor B cell–derived leukemia with 100% penetrance (4, 5). Inducible deletion of *Tet1* and *Tet2* using *Mx1-Cre* promoted the development of acute lymphoblastic leukemia derived from precursor B cells, and global loss of *Tet1* caused B cell lymphomas with an extended latency (6). In humans, *TET2* mutations are frequently observed in diffuse large B cell lymphoma, a malignancy derived from germinal center (GC) B cells (7, 8), suggesting that TET proteins may regulate mature B cell function. However, because of the pleiotropic functions of TET proteins, studies of TET-mediated gene regulation are best performed in systems where TET genes are deleted acutely rather than during development.

After their development in the bone marrow, mature B cells migrate to peripheral lymphoid tissues where they encounter antigen and follicular T helper cells in GCs and participate in the generation of functional immune responses (9). In GCs, B cells diversify the variable regions of immunoglobulin (Ig) chains in a process known as somatic hypermutation (SHM) and also undergo class switch recombination (CSR) to replace the immunoglobulin M (IgM) constant region with those of other isotypes (IgG1, IgA, etc.). Both CSR and SHM are orchestrated by the enzyme AID (activation-induced cytidine deaminase, encoded by *Aicda*) (10–12). AID promotes CSR and SHM by generating DNA double-strand breaks at Ig switch regions and point mutations at Ig variable regions, respectively (13). Because of its high mutagenic potential (14, 15), AID expression is normally restricted to activated B cells and is tightly regulated.

Here, we investigated the role of TET proteins during mouse B cell activation by mapping 5hmC distribution genome-wide and integrating the data with previous studies of transcriptional and epigenetic changes during B cell activation (16, 17). We deleted the *Tet2* and *Tet3* genes acutely using Cre^{ERT2} to avoid secondary effects caused by prolonged TET deficiency during differentiation. We show that TET2 and TET3 regulate CSR by controlling the activation-induced up-regulation of AID mRNA and protein and that they act downstream of the basic region/leucine zipper (bZIP) transcription factor BATF (basic leucine zipper transcription factor, ATF-like), which is induced during B cell activation with more rapid kinetics than *Aicda* and binds concomitantly with TET proteins to two TET-responsive elements in the *Aicda* locus, *TetE1* and *TetE2*. Our study demonstrates the role of TET proteins in CSR in activated B cells and provides a detailed description of the general mechanism whereby TET proteins influence cell activation and differentiation.

RESULTS

B cell activation promotes genome-wide deposition of 5hmC

We immunoprecipitated genomic DNA with antibodies to cytosine-5-methylenesulfonate (CMS-IP) (18, 19) to analyze the kinetics of 5hmC deposition in murine B cells activated with lipopolysaccharide (LPS) and interleukin-4 (IL-4), a well-characterized in vitro system for studying CSR (Fig. 1A). The vast majority of 5hmC-marked regions (~160,000) were shared between pre- and postactivated B cells (Fig. 1B and fig. S1A). Of the ~9500 differentially hydroxymethylated regions (DhmRs) in 72-hour-activated B cells versus naïve B cells, the majority (8454) had increased 5hmC ($DhmR^{72h\text{-}up}$), whereas a much smaller number (928) had decreased 5hmC ($DhmR^{down}$) (Fig. 1, B and C). DhmRs were typically located more than 10 kb from the closest transcription start site (TSS) (fig. S1B), and their 5hmC levels progressively changed with time after activation [$DhmR^{72h\text{-}up}$ (Fig. 1D) and $DhmR^{72h\text{-}down}$ (fig. S1C)].

The oxi-mC produced by TET proteins are known intermediates in DNA demethylation (2, 20). To relate 5hmC to changes in DNA methylation, we compared 5hmC distribution in naïve and 72-hour-activated B cells with published whole-genome bisulfite sequencing (WGBS) data on B cells activated for 48 hours under similar conditions (17). Although WGBS cannot distinguish 5mC from 5hmC (21), 5hmC is typically a small fraction (1 to 10%) of 5mC (22); thus, we refer to the WGBS signal as “DNA methylation” here. Most (1097 of 1168, 94%) differentially methylated regions (DMRs) were demethylated at 48 hours and marked by 5hmC (fig. S1, D and E). Regions that showed increased 5hmC at 24, 48, and 72 hours ($DhmR^{24h\text{-}up}$, $DhmR^{48h\text{-}up}$, and $DhmR^{72h\text{-}up}$) also showed decreased DNA methylation (Fig. 1E and fig. S1F). Overall, regions of 5hmC deposition correspond to regions of DNA hypomethylation during B cell activation, as expected from the well-established role of 5hmC as an intermediate in DNA demethylation. Motif enrichment analysis of the 8454 $DhmR^{72h\text{-}up}$ and 1097 $DMR^{48h\text{-}down}$ regions showed that both were enriched in consensus binding sequences for transcription factors of the nuclear factor κB (NF-κB) (Rel homology domain) and bZIP families, as well as for “composite” IRF:bZIP motifs (Fig. 1F and fig. S1G) (23–25).

To discern the relationship between 5hmC and enhancers, we stratified naïve and activated B cell enhancers, defined by H3K4 monomethylation (H3K4me1), on the basis of the level of H3K27 acetylation (H3K27Ac), a modification that tracks with enhancer activity (26). 5hmC was most highly enriched at active ($H3K4me1^+$ $H3K27Ac^+$) relative to poised ($H3K4me1^+$ $H3K27Ac^-$) enhancers (Fig. 1G). Moreover, more than 75% of previously identified superenhancers in activated B cells, defined by H3K27Ac, overlapped with at least one $DhmR^{72h\text{-}up}$ region (Fig. 1H) (27): For instance, a 3′ distal element at the *Ccr4* locus showed activation-dependent gain of 5hmC and H3K27Ac, associated with concomitant loss of methylation at specific CpGs and increased mRNA expression (Fig. 1, I and J). 5hmC was also associated with accessible chromatin defined by ATAC-seq (assay for transposase-accessible chromatin using sequencing) (4, 5, 28) (see below), and kinetic analysis of active enhancers showed that 5hmC levels correlated with enhancer activity (fig. S1H). Together, our data show that 5hmC modification and DNA demethylation correlate with enhancer activity during B cell activation.

Comparison of wild type and *Tet2/3* double-deficient B cells identifies TET-responsive regulatory elements

TET2 and TET3 are the two major TET proteins expressed in B cells (Fig. 2A). To evaluate the role of TET proteins in regulating B cell function, we treated Cre^{ERT2} $Tet2^{fl/fl}$ $Tet3^{fl/fl}$ $Rosa26\text{-}YFP^{LSL}$ for 5 days with tamoxifen to delete *Tet2* and *Tet3* (double knockout, DKO). $Tet2^{fl/fl}$ *Tet3fl/f l* $Rosa26\text{-}YFP^{LSL}$ wild-type (WT) mice were used as controls; YFP reports Cre expression. B cells were isolated and activated with LPS and IL-4 (Fig. 2B). *Tet2* and *Tet3* were both efficiently deleted in B cells (Fig. 2C), and the YFP^+ cells showed similar frequencies of mature splenic follicular B cells (fig. S2, A and B).

Global 5hmC levels were similar in WT and *Tet2/3* DKO B cells before activation but showed a perceptible decrease by 48 hours after activation, consistent with passive loss of 5hmC as a function of cell division (fig. S2C) (2, 20). Starting at 48 hours, 5hmC levels were substantially lower in *Tet2/3* DKO compared with WT B cells, indicating that TET2 and TET3 actively oxidize 5mC to 5hmC during B cell activation (fig. S2C). Around 2300 5hmC–enriched regions were significantly different between WT and DKO at 72 hours of activation, with substantially more regions gaining 5hmC in control compared with *Tet2/3* DKO B cells (Fig. 2, D and E); most were located >10 kb from the nearest TSS (fig. S2D). Of the 2139 “TET-regulated” DhmRs with higher 5hmC in WT compared with *Tet2/3* DKO B cells (“WT > DKO DhmR”), 2020 (94.4%) significantly overlapped with $DhmR^{72\text{-}up}$ regions; most showed decreased DNA methylation at their centers (fig. S2E) and were enriched for RHD, bZIP, and composite IRF:bZIP motifs (Fig. 2F).

TET2 and TET3 regulate Ig CSR

To assess the effect of *Tet2/3* deletion on the antibody response in vivo, we treated $Tet2^{fl/fl}$ $Tet3^{fl/fl}$ *Rosa26-LSL-YFP* Cre^{ERT2} and control mice with tamoxifen before immunization with 4-hydroxy-3-nitrophenylacetyl–conjugated ovalbumin (NP-OVA) (Fig. 3A). Acute deletion of *Tet2/3* resulted in increased numbers of total cells and B cells in draining popliteal lymph nodes by day 7 after immunization (fig. S3A), consistent with our previous observations that *Tet2/3* deficiency results in increased cell survival and/or proliferation

(28). The overall percentage of GC B cells ($CD19^+$ $GL7^+$ Fas^+) was similar between WT and DKO (gated on YFP^+) (Fig. 3, B and C), but there was a significant increase in the frequency of NP-specific B cells (Fig. 3D). There was also a moderate (~25%) decrease in GL7 MFI in *Tet2/3 DKO* GC B cells compared with WT control GC B cells (fig. S3B), indicating that although TET proteins are, in general, important for cell differentiation, acute deletion of *Tet2/3* in B cells had only a limited effect on GC B cell differentiation. Because acute *Tet2/3* deletion using the Cre^{ERT2} system affects multiple cell types, we did not investigate the in vivo B cell phenotype further in $Tet2^{fl/fl}$ $Tet3^{fl/fl}$ Cre^{ERT2} $Rosa26$ YFP^{LSL} mice. The most notable phenotype in these mice, however, was the consistent decrease in CSR from IgM to IgG1 (Fig. 3, E and F), demonstrating a role for TET proteins in regulating antibody responses in vivo, particularly the CSR.

To determine whether the CSR phenotype was B cell intrinsic, B cells from tamoxifen-treated mice were labeled with a proliferation-tracking dye (CellTrace Violet) and activated with LPS and IL-4 for 4 days (Fig. 3G). Consistent with the CSR defect in vivo, IgG1 switching in *Tet2/3* DKO B cells in vitro was consistently lower relative to WT B cells (Fig. 3, H and I). The impaired CSR in *Tet2/3* DKO was not due to Cre activity (fig. S3C); the defect was cell intrinsic based on mixing experiments (fig. S3D); and the difference was not due to altered proliferation (Fig. 3H and fig. S3E). Correlating with the decrease in CSR, the expression of circular γ1 transcript was decreased in *Tet2/3* DKO B cells (Fig. 3J). Furthermore, CSR to IgA was also decreased in *Tet2/3* DKO relative to WT B cells (Fig. 3, K to N). The loss of *Tet2/3* also resulted in a decrease in the differentiation of $CD138^+$ plasma blasts/cells after in vitro activation (fig. S3F). Reconstitution of *Tet2/3* DKO B cells with the enzymatically active catalytic domain of mouse TET2 (Tet2CD) (29) restored CSR almost to control levels (fig. S3, H and I). An enzymatically inactive mutant of Tet2CD ($Tet2CD^{HxD}$) also partially restored CSR, suggesting that both TET enzymatic activity and scaffolding function have a role in CSR (fig. S3, G to I) (30). Together, these results indicate that *Tet2* and *Tet3* are required for optimal CSR both in vitro and in vivo.

Because the CSR defect in *Tet2/3* DKO B cells was ~50% of control, we asked whether deletion of all three TET proteins might have a more notable effect. Consistent with the very low expression of *Tet1* in mature B cells (Fig. 2A), the CSR defect in *Tet1/2/3 TKO* mice was comparable to that observed in *Tet2/3* DKO mice (fig. S3, J and K). These results indicate that TET2 and TET3 are the major TET proteins that regulate CSR in B cells.

TET2 and TET3 regulate expression of the cytidine deaminase AID

CSR is a highly regulated process and involves multiple pathways (31). RNA sequencing (RNA-seq) analysis identified a relatively small number of genes differentially expressed between WT and *Tet2/3* DKO B cells (fig. S4, A and B); among these was *Aicda*, which encodes AID, a protein essential for CSR. Quantitative reverse transcription polymerase chain reaction (qRT-PCR) and Western blot analyses confirmed a >50% decrease in *Aicda* mRNA in *Tet2/3* DKO relative to WT B cells after activation (Fig. 4, A and B, and fig. S4, C and D), a phenotype that resembled the dampened CSR in AID haploinsufficient mice (fig. S4, E to J) (32, 33). Although *Tet2* mRNA expression showed only minor changes in unstimulated versus stimulated B cells (Fig. 2A), Tet2 protein expression was low in

unstimulated and 24-hour-stimulated B cells, with increased expression observed at 48 hours after stimulation (fig. S4D). The late TET2 induction parallels the late kinetics of increase in 5hmC (Fig. 1C).

To determine whether the decrease in AID expression was fully responsible for the CSR defect, we expressed WT and catalytically inactive AID ($AID^{H56R/E58Q}$) (34) in WT and *Tet2/3* DKO B cells via retroviral transduction. Retroviral expression of catalytically active AID (AID^{WT}), but not inactive $AID^{H56R/E58Q}$, largely rescued the CSR defect in *Tet2/3* DKO B cells (Fig. 4, C and D, bottom panels). Similar to previous observations (12), expression of AID in WT cells also increased the frequency of $IgG1^+$ cells (Fig. 4, C and D, top left and middle panels). Because Tet2/3 were not required for expression of the μ and γ1 germline transcripts essential for CSR (fig. S4K), the bulk of the CSR defect in *Tet2/3* DKO B cells can be attributed to the decrease in expression of *Aicda* mRNA and AID protein, leading us to test the hypothesis that TET proteins control *Aicda* expression through distal regulatory element(s) of the *Aicda* gene.

Genome-wide analyses identify TET-responsive regulatory elements in the *Aicda* locus

Multiple conserved regulatory elements influence *Aicda* expression (fig. S5A), and their deletion markedly decreased *Aicda* expression in activated B cells (17, 35–37). Of these, the *Aicda* 5′ enhancer at −26 kb in the *Mfap5* gene, the intergenic 5′ enhancers, and the intron 1 enhancer noticeably gain H3K27Ac and lose 5mC upon activation and have been collectively termed the *Aicda* "superenhancer" (Fig. 5A, middle and bottom tracks) (17, 27).

Chromatin immunoprecipitation sequencing (ChIP-seq) for TET2 showed that each of these regulatory elements was occupied by TET2 in 72-hour-activated B cells (Fig. 5A, top two tracks). Among these, the −26-kb *Mfap5* intronic region and the −8-kb 5′ intergenic region (here termed *TetE2* and *TetE1*, respectively) were TET-regulated: B cell activation induced a TET-dependent increase in 5hmC (Fig. 5B), placing them in the category of WT > DKO DhmRs (Fig. 2, D and E). *TetE1* appears to be the prime target for TET2/3 due to its larger gain of 5hmC after activation (Fig. 5B). In contrast, regions such as the *Aicda* promoter were marked by 5hmC even before activation, indicating that the 5hmC at these regions was likely generated during a previous stage of B cell differentiation and then maintained until the emergence of naïve peripheral B cells.

To confirm the importance of the *TetE1* enhancer in *Aicda* regulation, we deleted the enhancer using CRISPR in CH12F3 cells, a B cell line that can class-switch from IgM to IgA upon activation with anti-CD40/IL-4/TGFβ (fig. S5, B and C). We tested four clones with homozygous deletions; all showed decreased expression of *Aicda* mRNA, and in three of these, there was almost no detectable CSR (fig. S5, D and E), confirming a previous report in the context of a bacterial artificial chromosome (BAC) transgene that *TetE1* was essential for *Aicda* expression (36). B cell activation also induced hydroxymethylation at the *IgH* locus, most notably upstream of the IgG1 promoter (fig. S5F). Given that *Tet2/3* DKO B cells expressed similar levels of IgG1 germline transcripts (fig. S4K) and that ectopic expression of AID could rescue the impairment of IgG1 CSR, the significance of TET-mediated DNA modification/demethylation at the *IgH* locus remains to be determined.

B cell activation induces strong H3K27Ac and DNA demethylation at *TetE1* (Fig. 5A). Because bisulfite sequencing does not distinguish 5mC from 5hmC, we used oxidative bisulfite sequencing (oxBS-seq) to assess the levels of 5mC, 5hmC, and unmodified C at *TetE1* in WT and *Tet2/3* DKO cells [neither BS-seq nor oxBS-seq distinguish unmodified C from 5fC and 5caC, but these modified bases are ~10-fold and ~100-fold less abundant than 5hmC (2)]. CpGs in both *TetE1* and the *Aicda* promoter displayed similar levels of 5mC and 5hmC before activation (Fig. 5C and fig. S5H; compare 0-hour panels). At 72 hours after activation, there was a substantial decrease in 5mC in WT B cells; in contrast, both *TetE1* and the *Aicda* promoter were methylated in *Tet2/3* DKO B cells (Fig. 5C, bottom panel; compare 72-hour panels). These results indicate that TET2 and TET3 regulate *Aicda* expression by binding to and depositing 5hmC at *TetE1* and *TetE2*.

TET2 and TET3 maintain chromatin accessibility at two *Aicda* TET-responsive elements, *TetE1* and *TetE2*

Active regulatory regions are typically found in accessible regions of chromatin (38) and are marked by 5hmC (4, 28). To assess the dynamics of chromatin accessibility, we performed ATAC-seq in B cells stimulated with LPS and IL-4. Activated B cells displayed progressive chromatin remodeling (fig. S6A). Regions with increased 5hmC after activation ($DhmR^{72h\text{-}up}$) also showed increased chromatin accessibility after activation and vice versa (fig. S7A; blue box-and-whisker plots).

To understand the relationship between TET function and chromatin accessibility, we performed ATAC-seq on WT and *Tet2/3* DKO B cells activated as in Fig. 3G. Of a total of ~28,000 accessible regions (fig. S6, B and C), only a minor fraction (~1.5%; 421 of 28,137) showed significant changes in accessibility between WT and *Tet2/3* DKO B cells, and the differences were observed late, at 72 hours after activation (fig. S6, B to D). Of the 292 potentially TET-regulated differentially accessible regions (DARs), defined as showing decreased accessibility in *Tet2/3* DKO compared with WT B cells (WT > DKO DARs), the majority were located distal to the TSS (fig. S7B) and a significant proportion of these (110 of 292, 37.7%) showed a TET2/3-dependent increase in 5hmC at 72 hours compared with unstimulated cells ($DhmR^{72up}$) (figs. S6C and S7C, top). In contrast, the 129 DKO > WT DARs that were less accessible in WT compared with *Tet2/3* DKO B cells and the 27,716 commonly accessible DARs were present in both TSS-proximal and TSS-distal regions and did not show significant changes in 5hmC (fig. S6C, middle and bottom panels, and fig. S7, B and C). Analysis of DNA methylation at 48 hours after activation showed that WT > DKO DARs were further demethylated after activation, whereas DKO > WT DARs were already substantially demethylated in naïve B cells and showed no further changes after activation (fig. S7D). Moreover, the WT > DKO DARs were enriched in bZIP and BATF:IRF motifs (fig. S7E), similarly to those in $DhmR^{72h\text{-}up}$ (Fig. 1F) and WT > DKO DhmRs (Fig. 2F). Together, these data support our previously observed correlation of 5hmC modification with changes in chromatin accessibility.

Focusing on the *Aicda* locus, we found that activation was associated with increased accessibility at the *Aicda* enhancers *TetE1* and *TetE2* (fig. S6D). The 5hmC modification continuously increased at these two elements until 72 hours, with a higher level of

deposition at *TetE1* (see Fig. 5B). In contrast, the time course of increase in chromatin accessibility was quite different at the two enhancers (fig. S6D): *TetE2* showed a rapid increase in accessibility at 24 hours after activation, whereas the time course of increase in *TetE1* accessibility was slower, matching that of 5hmC deposition (compare Fig. 5B and fig. S6D). Consistent with the increased accessibility, several chromatin remodelers and histone acetyltransferases, including BRG1, CHD4, p300, and, to a lesser extent, GCN5, were recruited to *TetE1* and *TetE2* in 24-hour-activated B cells (fig. S7F). We noticed a slight decrease in chromatin accessibility at *TetE1* and *TetE2* in *Tet2/3* DKO B cells compared with WT cells at 72 hours, suggesting that TET proteins are important for maintaining chromatin accessibility at these enhancers (fig. S6E). Loss of TET proteins had no significant effect on chromatin accessibility at the *IgH* locus (fig. S5G). Together, these data point to a consistent link between bZIP-family transcription factors, TET catalytic activity, and chromatin accessibility.

BATF acts upstream of TET at *Aicda* enhancers

Before enhancers are established during development, cell lineage specification, or activation, certain key transcription factors bind to nucleosome-associated regions and recruit chromatin remodeling complexes and histone-modifying enzymes to create active enhancers (26). To identify potential pioneer transcription factors for the *Aicda* locus, we took advantage of our previous motif enrichment analyses (Figs. 1F and 2F and fig. S1G). We had observed strong enrichment for consensus binding motifs for bZIP transcription factors, at regions that progressively gained 5hmC as a function of activation (Fig. 1F, $DhmR^{up}$), regions that lost DNA methylation upon activation (fig. S1G, $DMR^{48h\text{-}down}$), regions with higher 5hmC in WT compared with *Tet2/3* DKO B cells (Fig. 2F, WT > DKO DhmRs), and regions with higher accessibility in WT versus *Tet2/3* DKO B cells (fig. S7E, DAR^{72h} WT > DKO).

On the basis of these data, we focused on bZIP transcription factors expressed in activated B cells. Consistent with previous observations (39, 40), *Batf* mRNA and protein were induced after activation (Fig. 6A and fig. S8B) and their expression preceded that of *Aicda*, as expected if BATF regulated *Aicda* mRNA induction (figs. S8, A and B, and S4D). In contrast, expression of *Bach1* and AP-1 (Fos and Jun) family members was either low throughout (*Fosl1*, *Fosl2*, *JunD*, and *Bach1*) or moderate to high in unstimulated B cells, potentially because these cells contained a minor population of memory B cells that express high levels of Fos and Jun (fig. S8, C to E; and Immgen.org) (41). Given the kinetics, we examined the importance of BATF in subsequent experiments.

BATF is essential for T and B cells during humoral responses (39, 40), and *Batf*-KO B cells are defective in CSR (fig. S8F) (39, 40). Genome-wide analysis of Batf binding by ChIP-seq in 72-hour-activated WT and *Tet2/3* DKO B cells showed very few overall differences (fig. S8G), indicating that BATF functioned upstream or independently of TET enzymes. Nevertheless, one of two distinguishable sets of BATF ChIP-seq peaks (cluster 2 in Fig. 6B) was TET-regulated, because the peaks in this cluster showed a progressive TET2/3-dependent increase in 5hmC after activation (Fig. 6, B and C). In contrast, BATF peaks in cluster 1 showed no significant activation-dependent increase in 5hmC (Fig. 6B, top panel).

Overall, about one-third of regions with activation-induced 5hmC (DhmR$^{72\text{-up}}$) overlapped with BATF peaks (fig. S8H), indicating that in addition to BATF, other transcription factors also have a role in facilitating TET-mediated 5hmC generation at the *Aicda* locus. Despite this strong functional interaction, we did not observe a substantial direct protein-protein interaction between BATF and TET2 in coimmunoprecipitation experiments in which the effects of nucleic acids were excluded (fig. S8I), suggesting that the interaction is dependent on additional factors.

BATF bound strongly at the *TetE1* and *TetE2* enhancers in the *Aicda* locus and, to a lesser extent, to the −21-kb intergenic enhancer located between *TetE1* and *TetE2* (Fig. 6D, 72-hour WT and DKO; second and third tracks). Consistent with the lack of BATF expression in unstimulated cells, there was no enrichment of BATF occupancy at the *Aicda* enhancers at 0 hours (Fig. 6D, 0-hour WT; top track). This binding pattern resembles that of TET2 (Fig. 5A), as well as that of E2A and PU.1 (Fig. 6D) (42–44). Moreover, BATF and JUNB associated with *TETE1* and *TETE2* in a human B cell lymphoblast (fig. S8L), suggesting that the binding of BATF to these enhancers is evolutionarily conserved. To determine whether BATF acted upstream of TET, we analyzed 5hmC deposition at the TET-responsive element *TetE1* in WT and *Batf*-deficient B cells. We found unambiguously that the absence of BATF abolished activation-induced hydroxymethylation at *TetE1* (Fig. 6E). Our results are consistent with the hypothesis that BATF facilitates the recruitment of TET2 and/or TET3 to *TetE1* and *TetE2* and increases *Aicda* expression by promoting 5hmC modification and DNA demethylation at these upstream *Aicda* enhancers.

As mentioned above, BATF is essential for *Aicda* regulation. However, we cannot rule out the involvement of additional transcription factors, including other bZIP family members, in this process. Although IRF4 is required for *Aicda* expression and binds to *TetE1* (45, 46), 5hmC levels at *TetE1* were unaffected in *Irf4*-deficient B cells after LPS/IL-4 stimulation (fig. S8M). Thus, depending on cell type and conditions of stimulation, certain transcription factors preferentially function together with TET proteins, whereas others could be responsible for additional aspects of locus remodeling and gene expression.

DISCUSSION

TET proteins oxidize 5mC to 5hmC, a stable epigenetic mark and an intermediate in DNA demethylation. Because of the pleiotropic effects of TET proteins in cells, it has been challenging to address the specific roles of TET proteins by using TET-deficient mice. To circumvent this problem, we used the inducible tamoxifen-*Cre*^{ERT2} system to delete *Tet2* and *Tet3* in mature B cells. Our data show that TET2 and TET3 are required for efficient CSR. A primary mechanism involves TET-mediated regulation of the expression of *Aicda*, the essential DNA cytosine deaminase for CSR. BATF, potentially with other transcription factors, helps recruit TET proteins to two major TET-responsive regulatory elements that we have newly defined in the *Aicda* locus, *TetE1* and *TetE2*. TET2 and TET3 convert 5mC to 5hmC at these regulatory elements, leading to DNA demethylation, sustaining enhancer accessibility and augmenting *Aicda* expression.

The biological consequences of TET loss of function are determined by several factors: the time course of *Tet2* and *Tet3* gene deletion, the stability of TET2 and TET3 mRNA and protein, and the rate of cell division that determines the rate of passive (i.e., replication dependent) dilution of 5hmC. At each cell division, hemi-methylated CpGs are recognized by the DNMT1/UHRF1 maintenance DNA methyltransferase complex and converted back to symmetrically methylated CpGs, whereas hemi-hydroxymethylated CpGs are ignored and so are diluted by half (1, 2). Consequently, 5hmC is present at comparable levels in quiescent (nondividing) WT and *Tet2/3* DKO B cells, thus enabling us to study the effects of acute TET deletion in activated, proliferating B cells. The progressive replication-dependent loss of 5hmC and consequent dilution of both 5mC and 5hmC is likely to be required for optimal gene expression, explaining the long-standing observation that the induction of *Aicda* expression during B cell activation and the induction of cytokine genes during T helper 2 (T_H2) cell differentiation are both tightly coupled to cell division (47, 48).

An optimal level of AID is crucial to maintain the necessary balance between effective antibody immune responses and unintentional C > T mutations caused by AID-mediated DNA cytidine deamination. Although *Aicda* haploinsufficiency results in dampened antibody responses (fig. S4, E to J) (32, 33), uncontrolled *AICDA* expression is associated with B cell malignancies (49). Thus, the level and activity of AID are meticulously controlled by diverse mechanisms including a tight transcriptional regulatory program (50). At the *Aicda* locus, at least six regulatory elements have been identified (fig. S5A); five of them, located at distances ranging from −29 to +5 kb relative to the TSS, are collectively termed the *Aicda* superenhancer (17, 27). The enhancers at −26, −21, −8, and +13 kb are all necessary for inducing *Aicda* expression in activated B cells, on the basis of deletion of individual enhancers in mice and the CH12 B cell line (36, 37). Even in naïve B cells where *Aicda* is not expressed, the *Aicda* promoter is already highly enriched in 5hmC and the −21-, intronic, and +13-kb *Aicda* enhancers display 5hmC and H3K27Ac (fig. S5A). The 5hmC modification at the −26-, −21-, and +13-kb *Aicda* enhancers is apparent as early as the pro–B cell stage of B cell development (4), suggesting that TET-mediated 5hmC modification acts to “bookmark” regulatory elements necessary for proper gene expression in progeny cells after activation.

The vast majority of 5hmC-marked regions are present in common between naïve and activated mature B cells (this study) and between WT and TET-deficient invariant natural killer T cells (iNKT) cells (28), supporting the hypothesis that most 5hmC-marked regions in any given cell type were laid down during previous developmental stages and thus are constitutively modified. In contrast, activation-induced 5hmC modification occurs at only a few distal elements in B cells (Fig. 1C), and 5hmC levels at these elements correlate strongly with activation-induced increases in enhancer activity defined by H3K27Ac (Fig. 1G) (51). Moreover, the majority of previously described B cell superenhancers (17, 27) harbor at least one activation-induced 5hmC-modified regulatory element (Fig. 1H). In the particular case of *Aicda*, we identified activation-induced 5hmC modification at two major TET-responsive elements, *TetE1* and *TetE2*, both part of a superenhancer cluster located 5′ of the *Aicda* gene (Fig. 5A) (17, 27). 5hmC modification at these elements was apparent by 48 hours (Fig. 5B), preceding the marked up-regulation of *Aicda* mRNA at 72 hours (fig. S4C). *Tet2/3* deficiency almost eliminated the activation-induced 5hmC modification at both

enhancers and resulted in diminished expression of both *Aicda* mRNA and AID protein (Figs. 4, A and B, and 5B and fig. S4C). Thus, our in vitro data indicate that TET proteins and 5hmC are important for *Aicda* expression by enabling the *TetE1* and *TetE2* enhancers to function at full capacity. However, we cannot rule out that in addition to decreasing AID expression, TET deficiency affects CSR indirectly by impeding B cell differentiation in vivo.

Our data strongly suggest that the bZIP transcription factor BATF is a major bZIP transcription factor responsible for TET recruitment to the *Aicda* locus, consistent with the identification that the bZIP motif is the singularly most enriched motif that correlated with DNA demethylation after B cell activation in human (52). BATF is induced at the mRNA level before *Aicda* induction in activated B cells (Fig. 6A), and *Batf* deficiency in B cells is associated with a marked impairment of AID expression and CSR (39, 40). Although loss of TET2 and TET3 had no significant effect on global BATF binding (Fig. 6B and fig. S8G), BATF was required for 5hmC modification at *TetE1* (Fig. 6E). Composite bZIP:IRF motifs and AP-1 motifs that support BATF:JUN:IRF and BATF:JUN cooperation, respectively, were enriched in our genome-wide 5hmC, ATAC, and DNA methylation datasets (Figs. 1F and 2F and figs. S1G and S7E), consistent with previous findings that B cells lacking BATF or IRF4/IRF8 show impaired *Aicda* induction and CSR (39, 40, 45, 46, 53). We propose that together with additional transcription factors, BATF:JunB and BATF:IRF facilitate the recruitment of TET proteins as well as chromatin remodeling complexes to diverse enhancers including the *Aicda* enhancers *TetE1* and *TetE2* in activated B cells, thereby promoting enhancer accessibility, 5hmC deposition, and DNA demethylation. We note, however, that the phenotype of *Batf*-KO mice and B cells is considerably more severe than that of *Tet2/3* DKO mice and B cells. Thus, TET2/3 proteins likely function as one of several modulators of BATF function in CSR.

Our data emphasize the utility of 5hmC mapping for easy, one-step analysis of transcriptional and epigenetic landscapes in any cell type of interest. 5hmC is a quintessential epigenetic modification that is most highly enriched at active enhancers and in the gene bodies of highly transcribed genes; thus, the relative levels of 5hmC at enhancers and gene bodies provide good estimates of enhancer function and the magnitude of transcription, respectively (51). 5hmC mapping by CMS-IP sufficed to identify all known enhancers in the *Aicda* locus, in a manner that was superior to both H3K27Ac and TET2 ChIP-seq and changes in 5hmC identified enhancers relevant to any particular process of cell activation or differentiation separately from all enhancers in the genome. Given its high chemical stability, the fact that its measurement requires only purified DNA and the availability of methods for its sensitive and specific detection, 5hmC is an appealing epigenetic mark for studying gene regulation. Overall, 5hmC distribution provides information analogous to that from ATAC-seq and ChIP-seq for enhancer histone modifications, and moreover requires only DNA and not live cells, effectively providing a transcriptional history of any given cell type written in DNA. If the genome is akin to an encyclopedia, 5hmC highlights those entries most relevant to a particular biological process.

MATERIALS AND METHODS

Study design

The aim of this study was to characterize the function of TET enzymes and TET-mediated 5hmC modification in regulating B cell function. The genome-wide modification of 5hmC was analyzed as a function of time after B cell activation in vitro. To analyze the role of TET proteins in B cells in vitro and in vivo, *Tet2* and *Tet3* were acutely deleted using a tamoxifen-inducible system. The impact of TET loss of function on B cells was analyzed by flow cytometry, RNA-seq, and ATAC-seq. Potential TET-regulated regulatory elements and the transcription factors involved were identified on the basis of integrative genome-wide analyses.

Mice

Tet2$^{fl/fl}$ and *Tet3*$^{fl/fl}$ mice were generated as previously described (54, 55). C57BL/6J (000664), Ubc-Cre^{ERT2} (008085; located at *Ndor1* locus; described as Cre^{ERT2} herein), Rosa26-LSL-EYFP (006148), and AID-Cre (007770) were obtained from the Jackson Laboratory. The LSL (*LoxP*-STOP-*LoxP*) cassette in Rosa26-LSL-EYFP mice contains a strong transcriptional stop flanked by two LoxP sites and was used as an indicator of the Cre activity. All mice used were 8 to 16 weeks in the C57BL/6 background and kept in a specific pathogen-free animal facility at La Jolla Institute and were used according to protocols approved by the Institutional Animal Care and Use Committee. To induce Cre^{ERT2}-mediated deletion, we intraperitoneally injected Cre-expressing and control mice with 2 mg of tamoxifen (Sigma) dissolved in 100 μl of corn oil (Sigma) daily for 5 days. H. Singh provided splenocytes from *Cd19-Cre Irf4-flox* mice.

B cell isolation and CSR

B cells were isolated with the EasySep Mouse B cell isolation kit (STEMCELL Technologies, Canada) from splenocytes. To induce CSR from IgM to IgG1, B cells (5×10^5 to 1×10^6 cells/ml) were activated with LPS (25 μg/ml) from *Escherichia coli* O55:B5 (Sigma, St. Louis, MO) and rmIL-4 (10 ng/ml) at 37°C (5% CO_2). For IgA switching, cells were activated with anti-CD40 (1 μg/ml, clone 1C10, BioLegend), rmIL-4 (10 ng/ml, Peprotech), rmIL-5 (10 ng/ml, Peprotech), and rhTGFβ1 (transforming growth factor β 1, 1 ng/ml). Media were composed of RPMI 1640 (Thermo Fisher Scientific, Waltham, MA, USA) supplemented with 10% FBS, 1× minimum essential medium (MEM) non-essential amino acids, 10 mM Hepes, 2 mM Glutamax, 1 mM sodium pyruvate, 55 μM 2-mercaptoethanol, and gentamicin (50 μg/ml) (all from Thermo Fisher Scientific, Waltham, MA, USA). To enhance *Cre^{ERT2}*-mediated deletion, we cultured cells from *Cre^{ERT2}* mice in the presence of 1 μM 4-hydroxytamoxifen (Tocris). All cytokines used above were from PeproTech (Rocky Hill, NJ, USA).

Immunization

For NP-OVA (Biosearch) immunization, the hapten-conjugated protein was diluted to 1 mg/ml in PBS, mixed with 1 volume of Alhydrogel (Invivogen), and injected into hind footpads (10 μg in 20 μl per injection). GC response was analyzed 7 days later, and the two

draining popliteal lymph nodes were pooled for analysis. Hapten-specific B cells were identified by positive staining with NP-phycoerythrin (Biosearch Technologies).

Retroviral transduction and two-step CSR

Retrovirus was produced by transfecting PlatE cells with murine stem cell virus–based retroviral vectors and pCL-Eco. Naïve B cells were stimulated with $F(ab')_2$ goat antimouse IgM (5 μg/ml; Jackson ImmunoResearch) and LPS (10 μg/ml) at 1×10^6 cells/ml for 24 to 48 hours. Note that this stimulation condition inhibits CSR, and AID expression was delayed (56). Retrovirus was added to the cells in the presence of 20 mM Hepes and Polybrene (0.8 μg/ml; Millipore) and centrifuged at 3000 rpm at 32°C for 90 min. Cells were transferred back to a 37°C, 5% CO_2 incubator for another 24 hours. To induce CSR, cells were washed once with warm media and activated with LPS and IL-4 as above for 48 hours. Under this condition, CSR was inhibited and started to class-switch only after LPS/IL-4 activation.

Flow cytometry

Primary cells and in vitro cultured cells were stained in fluorescence-activated cell sorting (FACS) buffer (1% bovine serum albumin, 1 mM EDTA, and 0.05% sodium azide in PBS) with indicated antibodies for 30 min on ice. Cells were washed and then fixed with 1% paraformaldehyde (diluted from 4% with PBS; Affymetrix) before flow cytometric analysis using FACS Canto II and FACS LSR II (BD Biosciences). Antibodies and dye were from BioLegend, eBioscience, and BD Pharmingen. Data were analyzed with FlowJo (FlowJo LLC, Ashland, OR, USA).

Immunoblotting

Proteins isolated from B cells with radioimmunoprecipitation assay (RIPA) buffer were resolved using NuPAGE 4 to 12% bis-tris gel (Thermo Fisher Scientific) and transferred from gel to polyvinylidene difluoride membrane using Wet/Tank Blotting Systems (Bio-Rad). Membrane was blocked with 5% nonfat milk (Bob's Red Mill) in TBSTE buffer [50 mM tris-HCl (pH 7.4), 150 mM NaCl, 0.05% Tween 20, and 1 mM EDTA] and incubated with indicated primary antibodies, followed by secondary antibodies conjugated with horseradish peroxidase (HRP), and signal was detected with enhanced chemiluminescence reagents and x-ray film.

Coimmunoprecipitation

Coimmunoprecipitation was performed similar to previously described (4). Briefly, in vitro activated B cells (48 hours) were washed twice with cold PBS and then resuspended in swelling buffer [5 mM tris (pH 7.5), 2 mM $MgCl_2$, and 3 mM $CaCl_2$] at 10×10^6 cells/ml. After 10 min on-ice incubation, cells were pelleted (400*g*, 5 min) and resuspended in swelling buffer with 10% glycerol. An equal volume of lysis buffer (1% NP-40 in swelling buffer with 10% glycerol) was added to the cells with constant mixing. Cells were incubated on ice for 5 min, pelleted (400*g*, 5 min) and resuspended in buffer C [10 mM Hepes (pH 7.9), 400 mM NaCl, and 1 mM EDTA] supplemented with benzonase (500 U/ml; Sigma) at 10×10^6 cells/ml, and incubated at 4°C for 30 min with constant mixing. Debris was removed by centrifuge at 13,000 rpm for 10 min, and supernatant (nuclear fraction) was

recovered. An equal volume of 2× conversion buffer [10 mM tris-HCl (pH 7.5), 280 mM NaCl, 1 mM EDTA, 1 mM EGTA, 0.2% sodium deoxycholate, and 0.2% Triton X-100] was added to the nuclear proteins. For immunoprecipitation, 10 μg of rabbit anti-TET2 (Abcam) or control rabbit Ig (Santa Cruz Biotechnology) was added to the nuclear extract with 30 μl of protein A Dynabeads (Thermo Fisher Scientific) in the presence of benzonase (500 U/ml) and ethidium bromide (10 μg/μl), both of which inhibit the indirect binding between nuclear proteins via DNA. Reaction was carried out overnight at 4°C and washed three times with RIPA buffer without SDS [50 mM tris-HCl (pH 8.0), 150 mM NaCl, 1 mM EDTA, 0.5% sodium deoxycholate, and 1% NP-40]. Proteins were eluted from beads by heating at 70°C for 10 min with 1× LDS (lithium dodecyl sulfate) sample buffers (Thermo Fisher Scientific) with 10% 2-mercaptoethanol (Sigma). Immunoprecipitated proteins were analyzed as described above using immunoblotting with Rabbit TrueBlot Anti-Rabbit IgG HRP (Rockland) as secondary antibody.

RNA extraction, cDNA synthesis, and qRT-PCR

Total RNA was isolated with RNeasy Plus Kit (Qiagen, Germany) or with Trizol (Thermo Fisher Scientific, Waltham, MA, USA) following the manufacturers' instructions. cDNA was synthesized using SuperScript III reverse transcriptase (Thermo Fisher Scientific), and qRT-PCR was performed using FastStart Universal SYBR Green Master Mix (Roche, Germany) on a StepOnePlus Real-time PCR system (Thermo Fisher Scientific). Gene expression was normalized to *Gapdh*. Primers are listed in table S3.

BS and oxBS sequencing

The BS and oxBS procedures were performed as previously described (22). Briefly, three PCR products containing C, mC, or hmC pertaining to different regions of λ phage genome were used as spike-ins at a ratio of 1:200 of the genomic DNA. A total of 1.5 μg of genomic DNA mixed with spike-ins was ethanol-precipitated, of which 1 μg of the DNA was oxidized with potassium perruthenate ($KRuO_4$; Sigma) before BS treatment (for oxBS) using the MethylCode Bisulfite Conversion Kit (Thermo Fisher Scientific), and 0.5 μg of DNA was directly used for BS treatment. The BS- and oxBS-treated DNA were amplified using respective PCR primers as well as primers specific to the spike-in PCR products with KAPA Uracil$^+$ PCR mix (Roche). The amplified products were pooled and libraries were prepared using the NEB Ultra II library preparation kit (NEB) according to the manufacturer. The libraries were sequenced paired-end 250 base pairs (bp) by 250 bp using MiSeq with the MiSeq reagent kit v2 (500 cycles; Illumina). Primers are listed in table S3.

Genome-wide 5hmC mapping by CMS-IP

Techniques for immunoprecipitation of DNA with antibodies are plagued by the fact that Igs nonspecifically immunoprecipitate DNA sequences containing CA and other DNA repeats (57). However, CMS is a derivative formed only after the reaction of 5hmC with sodium bisulfite, and anti-CMS antibodies recognize CMS with strong sensitivity and selectivity (19). Lentini *et al.* showed that the CMS-IP method is free of the nonspecific background of immunoprecipitation of DNA repeats, most likely because bisulfite treatment results in C > T conversions and/or single-stranded, as supposed to double-stranded, DNA was used for IP (57).

CMS-IP was performed essentially as previously described (4, 18, 19). Briefly, genomic DNA isolated from naïve and activated B cells was spiked with unmethylated lambda phage cI857 Sam7 DNA (Promega, Madison, WI, USA) and a PCR amplicon from a puromycin-resistant gene at a ratio of 200:1 and 100,000:1, respectively. DNA (5 to 10 μg in 130 μl tris-EDTA buffer) was sheared with a Covaris E220 using microTUBE for 4 min. DNA was cleaned up with Ampure XP beads, processed with NEBNext End Repair and A-tail Modules (NEB, Ipswich, MA, USA), and ligated to methylated Illumina adaptors (NEB). DNA was then bisulfite-treated (MethylCode, Thermo Fisher Scientific), denatured, and immunoprecipitated with anti-CMS serum (in-house) and a mixture of protein A and G Dynabeads (Thermo Fisher Scientific). Because our goal for this study was to identify regions that undergo significant activation-induced 5hmC modification after LPS + IL-4 stimulation, we normalized the data within each sample using total sequencing read counts for each individual time point, without using 5hmC-containing oligonucleotides as spike-ins to take into account the progressive dilution of 5hmC that occurs as a function of cell division (fig. S2C). Libraries for immunoprecipitated DNA were generated by PCR with barcoded primers (NEBNext Multiplex Oligos for Illumina; NEB) for 15 cycles using KAPA HiFi HotStart Uracil+ ReadyMix (Roche), followed by a cleanup with Ampure XP beads (Beckman Coulter), and sequenced with a HiSeq 2500 (Illumina, San Diego, CA, USA) with paired-end 50-bp reads.

Locus-specific analysis of 5hmC with Aba SI–qPCR

Genomic DNA (200 ng) was treated with T_4 β-glucosyltransferase (Thermo Fisher Scientific) in the presence of UDP-glucose to glycosylate 5hmC at 37°C overnight. Half of the reaction was digested with Aba SI (NEB), which is specifically active for glycosylated 5hmC for 4 hours at 25°C followed by 15 min at 65°C to inactivate enzymes. The uncut sample was processed as above without the addition of Aba SI. Equal amount of DNA from the above reactions was used as template for RT-PCR as described for RNA qRT-PCR using primers TetE1-CMS-qF and TetE1-CMS-qR. Data shown were normalized to the signal obtained from WT naïve B cells. To monitor the degree of digestion, samples were spiked in 1 pg of control DNA with a single 5hmC-modified CpG (EpiMark 5hmC and 5mC Analysis Kit; NEB). The relative amount of 5hmC was calculated by the percentage of decrease in qPCR signals in the digested portion relative to the undigested portion. As a control to monitor nonspecific digestion, a genomic region containing CpG motifs but without 5hmC modification in B cells (*Foxp3 CNS2*) was amplified with Foxp3-CNS2-qF and Foxp3-CNS2-qR. Primers are listed in table S3.

DNA dot blot

DNA dot blot was performed as previously described (4, 22). To analyze 5hmC abundance, genomic DNA was treated with sodium bisulfite as above. DNA was diluted twofold serially with TE buffer, denatured in 0.4 M sodium hydroxide and 10 mM EDTA at 95°C for 10 min, and then immediately chilled on ice. An equal volume of ice-cold 2 M ammonium acetate (pH 7.0) was added and incubated on ice for 10 min. Denatured DNA were spotted on a nitrocellulose membrane using a Bio-Dot apparatus (Bio-Rad), washed with 2× SSC buffer (300 mM NaCl and 30 mM sodium citrate), and baked in a vacuum oven at 80°C for 2 hours. To detect CMS, we rehydrated membrane with TBSTE buffer and blocked it with 5%

nonfat milk (Bob's Red Mill) in TBSTE buffer. CMS was detected with primary rabbit anti-CMS antisera (in-house) following the procedures above for immunoblotting.

Chromatin immunoprecipitation sequencing

ChIP was performed as described before (4). Briefly, cells were fixed with 1% formaldehyde (Thermo Fisher Scientific) at room temperature for 10 min at 1×10^6 cell/ml in media, quenched with 125 mM glycine, and washed twice with ice-cold PBS. Cells were pelleted, snap-frozen with liquid nitrogen, and stored at −80°C until use. For TET2-ChIP, activated cells were centrifuged at 250*g* for 5 min, and cell pellets were resuspended in 37°C PBS with 2 mM disuccinimidyl glutarate to cross-link proteins for 30 min at room temperature. Formaldehyde was added to a final concentration of 1%, and the cells were incubated at room temperature for 10 min with nutation. Quenching and cell storage were performed as above. To isolate nuclei for sonication, cell pellets were thawed on ice, lysed with lysis buffer [50 mM Hepes (pH 7.5), 140 mM NaCl, 1 mM EDTA, 10% glycerol, 0.5% NP-40, and 0.25% Triton X-100] for 10 min at 4°C with rotation, and washed once with washing buffer [10 mM tris-HCl (pH 8.0), 200 mM NaCl, 1 mM EDTA, and 0.5 mM EGTA] and twice with shearing buffer [10 mM tris-HCl (pH 8.0), 1 mM EDTA, and 0.1% SDS]. Nuclei were resuspended in 1 ml of shearing buffer and sonicated with Covaris E220 using 1-ml milliTUBE (Covaris, Woburn, MA) for 18 to 20 min (duty cycle, 5; intensity, 140 W; cycles per burst, 200). After sonication, insoluble debris was removed by centrifugation at 20,000*g*. Buffer for chromatin was adjusted with 1 volume of 2× conversion buffer [10 mM tris-HCl (pH 7.5), 280 mM NaCl, 1 mM EDTA, 1 mM EGTA, 0.2% sodium deoxycholate, 0.2% Triton X-100, and 1% Halt protease inhibitors with (for H3K27Ac) or without (for BATF, TET2) 0.1% SDS]. Chromatin was precleared with washed protein A (Thermo Fisher Scientific) for 2 hours and incubated with antibodies and protein A Dynabeads overnight (all procedures were at 4°C with rotation). For H3K27Ac ChIP, bead-bound chromatin was washed twice with RIPA buffer [50 mM tris-HCl (pH 8.0), 150 mM NaCl, 1 mM EDTA, 0.5% sodium deoxycholate, 1% NP-40, and 0.1% SDS], once with high-salt wash buffer [50 mM tris-HCl (pH 8.0), 500 mM NaCl, 1 mM EDTA, 1% NP-40, and 0.1% SDS], and once with TE [10 mM tris-HCl (pH 8.0) and 1 mM EDTA]. For BATF ChIP, all wash buffers were as above but without SDS. For TET2 ChIP, beads were washed three times with RIPA buffer without SDS and once with TE. Chromatin was eluted from beads with elution buffer (100 mM $NaHCO_3$, 1% SDS, and 1 mg/ml RNase A; Qiagen) twice for 30 min each at 37°C with constant shaking. NaCl and proteinase K (Ambion) were added to the eluted chromatin at concentrations of 250 mM and 0.5 mg/ml, respectively, and de-cross-linked at 65°C overnight with constant shaking. DNA was purified with Zymo ChIP DNA Clean & Concentrator Capped Column (Zymo Research, Irvine, CA, USA). Library was prepared with NEB Ultra II Library Prep Kit (NEB) following the manufacturer's instruction and was sequenced on an Illumina HiSeq 2500 (single-end 50-bp reads).

ATAC-seq

Procedures were as previously described (4). Briefly, 50,000 cells were collected by centrifugation and washed once with 50 μl of ice-cold PBS and centrifuged at 600*g* for 5 min at 4°C. Cell pellets were resuspended in 50 μl of cold lysis buffer [10 mM tris-HCl (pH 7.4), 10 mM NaCl, 3 mM $MgCl_2$, and 0.1% IGEPAL CA-630] and spun down immediately

at 500*g* for 10 min at 4°C. Supernatant was discarded and nuclei were resuspended in 50 μl of transposition reaction mix (25 μl of 1× TD buffer from Illumina, 2.5 μl of Tn5 transposase, and μl of H_2O), incubated at 37°C for 30 min, and DNA was purified with a Qiagen MinElute kit (Qiagen). Library was amplified with KAPA HiFi HotStart Real-time PCR Master Mix (Roche) using indexed primers and sequenced on an Illumina HiSeq 2500 (paired-end 50-bp reads).

RNA sequencing with Smart-seq

Smart-seq was performed as described previously (28, 58). Briefly, total RNA was isolated from naïve and activated B cells with Trizol (Thermo Fisher Scientific), and the integrity of the RNA was accessed with TapeStation RNA analysis ScreenTape or BioAnalyzer RNA Pico Kit (Agilent). Ten nanograms of RNA was reverse-transcribed using oligo-dT_{30} VN primer in the presence of Template Switching Oligo (TSO) with SuperScript II reverse transcriptase. cDNA was pre-amplified with IS PCR primers, and PCR products were cleaned up with Ampure XP beads. One nanogram of the PCR product was used to generate library using Nextera XT Library Prep Kit (Illumina), and tagmentated DNA was amplified for a 12-cycle PCR and purified with Ampure XP beads. Libraries were sequenced on an Illumina HiSeq 2500 with single-end 50-bp reads.

Statistical analyses

Statistical analyses and bar plots were performed and plotted with Prism 7 or R (v3.3.3). The bar graph and dot plots shown indicate mean and SE. Most experiments were analyzed using two-tailed unpaired *t* test or Wilcoxon rank-sum test, as indicated in the figure legends unless otherwise stated.

Supplementary Material

Refer to Web version on PubMed Central for supplementary material.

Acknowledgments:

We would like to thank U. Basu for providing the AID antibody; K. Yu for *Aicda*-KO CH12F3 cells; H. Singh for splenocytes from *Cd19-cre Irf4-flox* mice; P. Casali and H. Zan for discussions; L. Hempleman for assisting with animal experiments; C. Kim, L. Nosworthy, D. Hinz, and R. Simmons (LJI Flow Cytometry Core) for cell sorting; J. Day and N. Wlodychak (LJI Functional Genomics Center) for assistance with next-generation sequencing; and S. Bélanger for advice on immunization.

Funding: C.-W.J.L. was supported by a Cancer Research Institute Irvington Postdoctoral Fellowship and the Independent Investigator Fund (Kyowa Hakko Kirin/LJI). V.S. was supported by a Leukemia and Lymphoma Society Postdoctoral Fellowship (grant ID: 5463-18). D.S.-C. and E.G.A. were supported by the CONACYT/UCMEXUS fellowship from Mexico-US. This work was supported by the National Institutes of Health (NIH) grants R35 CA210043, R01 AI109842, and AI128589 (to A.R.) and R01 AI127642 (to D.G.S.). F.A. and A.C. were partially supported by Institute Leadership Funds from the LJI and by NIH grants R01 MH111267 and R35 GM128938. Purchase of the Illumina HiSeq 2500 and the BD FACSAria II was supported by equipment grants NIH S10OD016262 and NIH S10RR027366, respectively.

REFERENCES AND NOTES

1. Wu X, Zhang Y, TET-mediated active DNA demethylation: Mechanism, function and beyond. Nat. Rev. Genet 18, 517–534 (2017). [PubMed: 28555658]

2. Tsagaratou A, Lio C-WJ, Yue X, Rao A, TET methylcytosine oxidases in T cell and B cell development and function. Front. Immunol 8, 220 (2017). [PubMed: 28408905]

3. Lio C-W, Zhang J, González-Avalos E, Hogan PG, Chang X, Rao A, Tet2 and Tet3 cooperate with B-lineage transcription factors to regulate DNA modification and chromatin accessibility. eLife 5, e18290 (2016). [PubMed: 27869616]

4. Scott-Browne JP, Lio C-WJ, Rao A, TET proteins in natural and induced differentiation. Curr. Opin. Genet. Dev 46, 202–208 (2017). [PubMed: 28888139]

5. Orlanski S, Labi V, Reizel Y, Spiro A, Lichtenstein M, Levin-Klein R, Koralov SB, Skversky Y, Rajewsky K, Cedar H, Bergman Y, Tissue-specific DNA demethylation is required for proper B-cell differentiation and function. Proc. Natl. Acad. Sci. U.S.A 113, 5018–5023 (2016). [PubMed: 27091986]

6. Quivoron C, Couronné L, Della Valle V, Lopez CK, Plo I, Wagner-Ballon O, Do Cruzeiro M, Delhommeau F, Arnulf B, Stern M-H, Godley L, Opolon P, Tilly H, Solary E, Duffourd Y, Dessen P, Merle-Beral H, Nguyen-Khac F, Fontenay M, Vainchenker W, Bastard C, Mercher T, Bernard OA, TET2 inactivation results in pleiotropic hematopoietic abnormalities in mouse and is a recurrent event during human lymphomagenesis. Cancer Cell 20, 25–38 (2011). [PubMed: 21723201]

7. Schmitz R, Wright GW, Huang DW, Johnson CA, Phelan JD, Wang JQ, Roulland S, Kasbekar M, Young RM, Shaffer AL, Hodson DJ, Xiao W, Yu X, Yang Y, Zhao H, Xu W, Liu X, Zhou B, Du W, Chan WC, Jaffe ES, Gascoyne RD, Connors JM, Campo E, Lopez-Guillermo A, Rosenwald A, Ott G, Delabie J, Rimsza LM, Tay Kuang Wei K, Zelenetz AD, Leonard JP, Bartlett NL, Tran B, Shetty J, Zhao Y, Soppet DR, Pittaluga S, Wilson WH, Staudt LM, Genetics and pathogenesis of diffuse large B-cell lymphoma. N. Engl. J. Med 378, 1396–1407 (2018). [PubMed: 29641966]

8. Reddy A, Zhang J, Davis NS, Moffitt AB, Love CL, Waldrop A, Leppa S, Pasanen A, Meriranta L, Karjalainen-Lindsberg M-L, Nørgaard P, Pedersen M, Gang AO, Høgdall E, Heavican TB, Lone W, Iqbal J, Qin Q, Li G, Kim SY, Healy J, Richards KL, Fedoriw Y, Bernal-Mizrachi L, Koff JL, Staton AD, Flowers CR, Paltiel O, Goldschmidt N, Calaminici M, Clear A, Gribben J, Nguyen E, Czader MB, Ondrejka SL, Collie A, Hsi ED, Tse E, Au-Yeung RKH, Kwong Y-L, Srivastava G, Choi WWL, Evens AM, Pilichowska M, Sengar M, Reddy N, Li S, Chadburn A, Gordon LI, Jaffe ES, Levy S, Rempel R, Tzeng T, Happ LE, Dave T, Rajagopalan D, Datta J, Dunson DB, Dave SS, Genetic and functional drivers of diffuse large B cell lymphoma. Cell 171, 481–494.e15 (2017). [PubMed: 28985567]

9. De Silva NS, Klein U, Dynamics of B cells in germinal centres. Nat. Rev. Immunol 15, 137–148 (2015). [PubMed: 25656706]

10. Chandra V, Bortnick A, Murre C, AID targeting: Old mysteries and new challenges. Trends Immunol 36, 527–535 (2015). [PubMed: 26254147]

11. Vaidyanathan B, Chaudhuri J, Epigenetic codes programing class switch recombination. Front. Immunol 6, 405 (2015). [PubMed: 26441954]

12. Muramatsu M, Kinoshita K, Fagarasan S, Yamada S, Shinkai Y, Honjo T, Class switch recombination and hypermutation require activation-induced cytidine deaminase (AID), a potential RNA editing enzyme. Cell 102, 553–563 (2000). [PubMed: 11007474]

13. Alt FW, Zhang Y, Meng F-L, Guo C, Schwer B, Mechanisms of programmed DNA lesions and genomic instability in the immune system. Cell 152, 417–429 (2013). [PubMed: 23374339]

14. Casellas R, Basu U, Yewdell WT, Chaudhuri J, Robbiani DF, Di Noia JM, Mutations, kataegis and translocations in B cells: Understanding AID promiscuous activity. Nat. Rev. Immunol 16, 164–176 (2016). [PubMed: 26898111]

15. Robbiani DF, Nussenzweig MC, Chromosome translocation, B cell lymphoma, and activation-induced cytidine deaminase. Annu. Rev. Pathol 8, 79–103 (2013). [PubMed: 22974238]

16. Kieffer-Kwon K-R, Nimura K, Rao SSP, Xu J, Jung S, Pekowska A, Dose M, Stevens E, Mathe E, Dong P, Huang S-C, Ricci MA, Baranello L, Zheng Y, Tomassoni Ardori F, Resch W, Stavreva D, Nelson S, McAndrew M, Casellas A, Finn E, Gregory C, St Hilaire BG, Johnson SM, Dubois W, Cosma MP, Batchelor E, Levens D, Phair RD, Misteli T, Tessarollo L, Hager G, Lakadamyali M, Liu Z, Floer M, Shroff H, Aiden EL, Casellas R, Myc regulates chromatin decompaction and nuclear architecture during B cell activation. Mol. Cell 67, 566–578.e10 (2017). [PubMed: 28803781]

17. Kieffer-Kwon K-R, Tang Z, Mathe E, Qian J, Sung M-H, Li G, Resch W, Baek S, Pruett N, Grøntved L, Vian L, Nelson S, Zare H, Hakim O, Reyon D, Yamane A, Nakahashi H, Kovalchuk AL, Zou J, Joung JK, Sartorelli V, Wei C-L, Ruan X, Hager GL, Ruan Y, Casellas R, Interactome maps of mouse gene regulatory domains reveal basic principles of transcriptional regulation. Cell 155, 1507–1520 (2013). [PubMed: 24360274]

18. Huang Y, Pastor WA, Zepeda-Martinez JA, Rao A, The anti-CMS technique for genome-wide mapping of 5-hydroxymethylcytosine. Nat. Protoc 7, 1897–1908 (2012). [PubMed: 23018193]

19. Pastor WA, Pape UJ, Huang Y, Henderson HR, Lister R, Ko M, McLoughlin EM, Brudno Y, Mahapatra S, Kapranov P, Tahiliani M, Daley GQ, Liu XS, Ecker JR, Milos PM, Agarwal S, Rao A, Genome-wide mapping of 5-hydroxymethylcytosine in embryonic stem cells. Nature 473, 394–397 (2011). [PubMed: 21552279]

20. Pastor WA, Aravind L, Rao A, TETonic shift: Biological roles of TET proteins in DNA demethylation and transcription. Nat. Rev. Mol. Cell Biol 14, 341–356 (2013). [PubMed: 23698584]

21. Huang Y, Pastor WA, Shen Y, Tahiliani M, Liu DR, Rao A, The behaviour of 5-hydroxymethylcytosine in bisulfite sequencing. PLOS ONE 5, e8888 (2010). [PubMed: 20126651]

22. Yue X, Trifari S, Äijö T, Tsagaratou A, Pastor WA, Zepeda-Martinez JA, Lio C-WJ, Li X, Huang Y, Vijayanand P, Lähdesmäki H, Rao A, Control of Foxp3 stability through modulation of TET activity. J. Exp. Med 213, 377–397 (2016). [PubMed: 26903244]

23. Li P, Spolski R, Liao W, Wang L, Murphy TL, Murphy KM, Leonard WJ, BATF-JUN is critical for IRF4-mediated transcription in T cells. Nature 490, 543–546 (2012). [PubMed: 22992523]

24. Glasmacher E, Agrawal S, Chang AB, Murphy TL, Zeng W, Vander Lugt B, Khan AA, Ciofani M, Spooner CJ, Rutz S, Hackney J, Nurieva R, Escalante CR, Ouyang W, Littman DR, Murphy KM, Singh H, A genomic regulatory element that directs assembly and function of immune-specific AP-1-IRF complexes. Science 338, 975–980 (2012). [PubMed: 22983707]

25. Murphy TL, Tussiwand R, Murphy KM, Specificity through cooperation: BATF-IRF interactions control immune-regulatory networks. Nat. Rev. Immunol 13, 499–509 (2013). [PubMed: 23787991]

26. Calo E, Wysocka J, Modification of enhancer chromatin: What, how, and why? Mol. Cell 49, 825–837 (2013). [PubMed: 23473601]

27. Meng F-L, Du Z, Federation A, Hu J, Wang Q, Kieffer-Kwon K-R, Meyers RM, Amor C, Wasserman CR, Neuberg D, Casellas R, Nussenzweig MC, Bradner JE, Liu XS, Alt FW, Convergent transcription at intragenic super-enhancers targets AID-initiated genomic instability. Cell 159, 1538–1548 (2014). [PubMed: 25483776]

28. Tsagaratou A, Gonzaláz-Avalos E, Rautio S, Scott-Browne JP, Togher S, Pastor WA, Rothenberg EV, Chavez L, Lähdesmäki H, Rao A, TET proteins regulate the lineage specification and TCR-mediated expansion of iNKT cells. Nat. Immunol 18, 45–53 (2017). [PubMed: 27869820]

29. Ko M, An J, Bandukwala HS, Chavez L, Äijö T, Pastor WA, Segal MF, Li H, Koh KP, Lähdesmäki H, Hogan PG, Aravind L, Rao A, Modulation of TET2 expression and 5-methylcytosine oxidation by the CXXC domain protein IDAX. Nature 497, 122–126 (2013). [PubMed: 23563267]

30. Zhang Q, Zhao K, Shen Q, Han Y, Gu Y, Li X, Zhao D, Liu Y, Wang C, Zhang X, Su X, Liu J, Ge W, Levine RL, Li N, Cao X, Tet2 is required to resolve inflammation by recruiting Hdac2 to specifically repress IL-6. Nature 525, 389–393 (2015). [PubMed: 26287468]

31. Methot SP, Di Noia JM, Molecular mechanisms of somatic hypermutation and class switch recombination. Adv. Immunol 133, 37–87 (2017). [PubMed: 28215280]

32. Sernandez IV, de Yébenes VG, Dorsett Y, Ramiro AR, Haploinsufficiency of activation-induced deaminase for antibody diversification and chromosome translocations both in vitro and in vivo. PLOS ONE 3, e3927 (2008). [PubMed: 19079594]

33. Takizawa M, Tolarova H, Li Z, Dubois W, Lim S, Callen E, Franco S, Mosaico M, Feigenbaum L, Alt FW, Nussenzweig A, Potter M, Casellas R, AID expression levels determine the extent of cMyc oncogenic translocations and the incidence of B cell tumor development. J. Exp. Med 205, 1949–1957 (2008). [PubMed: 18678733]

34. Papavasiliou FN, Schatz DG, The activation-induced deaminase functions in a postcleavage step of the somatic hypermutation process. J. Exp. Med 195, 1193–1198 (2002). [PubMed: 11994424]

35. Crouch EE, Li Z, Takizawa M, Fichtner-Feigl S, Gourzi P, Montaño C, Feigenbaum L, Wilson P, Janz S, Papavasiliou FN, Casellas R, Regulation of AID expression in the immune response. J. Exp. Med 204, 1145–1156 (2007). [PubMed: 17452520]

36. Huong le T, Kobayashi M, Nakata M, Shioi G, Miyachi H, Honjo T, Nagaoka H, In vivo analysis of Aicda gene regulation: A critical balance between upstream enhancers and intronic silencers governs appropriate expression. PLOS ONE 8, e61433 (2013). [PubMed: 23613851]

37. Tran TH, Nakata M, Suzuki K, Begum NA, Shinkura R, Fagarasan S, Honjo T, Nagaoka H, B cell-specific and stimulation-responsive enhancers derepress Aicda by overcoming the effects of silencers. Nat. Immunol 11, 148–154 (2010). [PubMed: 19966806]

38. Roadmap Epigenomics Consortium, Kundaje A, Meuleman W, Ernst J, Bilenky M, Yen A, Heravi-Moussavi A, Kheradpour P, Zhang Z, Wang J, Ziller MJ, Amin V, Whitaker JW, Schultz MD, Ward LD, Sarkar A, Quon G, Sandstrom RS, Eaton ML, Wu Y-C, Pfenning AR, Wang X, Claussnitzer M, Liu Y, Coarfa C, Harris RA, Shoresh N, Epstein CB, Gjoneska E, Leung D, Xie W, Hawkins RD, Lister R, Hong C, Gascard P, Mungall AJ, Moore R, Chuah E, Tam A, Canfield TK, Hansen RS, Kaul R, Sabo PJ, Bansal MS, Carles A, Dixon JR, Farh K-H, Feizi S, Karlic R, Kim A-R, Kulkarni A, Li D, Lowdon R, Elliott G, Mercer TR, Neph SJ, Onuchic V, Polak P, Rajagopal N, Ray P, Sallari RC, Siebenthall KT, Sinnott-Armstrong NA, Stevens M, Thurman RE, Wu J, Zhang B, Zhou X, Beaudet AE, Boyer LA, De Jager PL, Farnham PJ, Fisher SJ, Haussler D, Jones SJM, Li W, Marra MA, McManus MT, Sunyaev S, Thomson JA, Tlsty TD, Tsai L-H, Wang W, Waterland RA, Zhang MQ, Chadwick LH, Bernstein BE, Costello JF, Ecker JR, Hirst M, Meissner A, Milosavljevic A, Ren B, Stamatoyannopoulos JA, Wang T, Kellis M, Integrative analysis of 111 reference human epigenomes. Nature 518, 317–330 (2015). [PubMed: 25693563]

39. Ise W, Kohyama M, Schraml BU, Zhang T, Schwer B, Basu U, Alt FW, Tang J, Oltz EM, Murphy TL, Murphy KM, The transcription factor BATF controls the global regulators of class-switch recombination in both B cells and T cells. Nat. Immunol 12, 536–543 (2011). [PubMed: 21572431]

40. Betz BC, Jordan-Williams KL, Wang C, Kang SG, Liao J, Logan MR, Kim CH, Taparowsky EJ, Batf coordinates multiple aspects of B and T cell function required for normal antibody responses. J. Exp. Med 207, 933–942 (2010). [PubMed: 20421391]

41. Heng TSP, Painter MW; The Immunological Genome Project Consortium, Elpek K, Lukacs-Kornek V, Mauermann N, Turley SJ, Koller D, Kim FS, Wagers AJ, Asinovski N, Davis S, Fassett M, Feuerer M, Gray DHD, Haxhinasto S, Hill JA, Hyatt G, Laplace C, Leatherbee K, Mathis D, Benoist C, Jianu R, Laidlaw DH, Best JA, Knell J, Goldrath AW, Jarjoura J, Sun JC, Zhu Y, Lanier LL, Ergun A, Li Z, Collins JJ, Shinton SA, Hardy RR, Friedline R, Sylvia K, Kang J, The Immunological Genome Project: Networks of gene expression in immune cells. Nat. Immunol 9, 1091–1094 (2008). [PubMed: 18800157]

42. Willis SN, Tellier J, Liao Y, Trezise S, Light A, O'Donnell K, Garrett-Sinha LA, Shi W, Tarlinton DM, Nutt SL, Environmental sensing by mature B cells is controlled by the transcription factors PU.1 and SpiB. Nat. Commun 8, 1426 (2017). [PubMed: 29127283]

43. Wöhner M, Tagoh H, Bilic I, Jaritz M, Poliakova DK, Fischer M, Busslinger M, Molecular functions of the transcription factors E2A and E2–2 in controlling germinal center B cell and plasma cell development. J. Exp. Med 213, 1201–1221 (2016). [PubMed: 27261530]

44. Gloury R, Zotos D, Zuidscherwoude M, Masson F, Liao Y, Hasbold J, Corcoran LM, Hodgkin PD, Belz GT, Shi W, Nutt SL, Tarlinton DM, Kallies A, Dynamic changes in Id3 and E-protein activity orchestrate germinal center and plasma cell development. J. Exp. Med 213, 1095–1111 (2016). [PubMed: 27217539]

45. Klein U, Casola S, Cattoretti G, Shen Q, Lia M, Mo T, Ludwig T, Rajewsky K, Dalla-Favera R, Transcription factor IRF4 controls plasma cell differentiation and class-switch recombination. Nat. Immunol 7, 773–782 (2006). [PubMed: 16767092]

46. Sciammas R, Shaffer AL, Schatz JH, Zhao H, Staudt LM, Singh H, Graded expression of interferon regulatory factor-4 coordinates isotype switching with plasma cell differentiation. Immunity 25, 225–236 (2006). [PubMed: 16919487]

47. Rush JS, Liu M, Odegard VH, Unniraman S, Schatz DG, Expression of activation-induced cytidine deaminase is regulated by cell division, providing a mechanistic basis for division-linked class

switch recombination. Proc. Natl. Acad. Sci. U.S.A 102, 13242–13247 (2005). [PubMed: 16141332]

48. Bird JJ, Brown DR, Mullen AC, Moskowitz NH, Mahowald MA, Sider JR, Gajewski TF, Wang CR, Reiner SL, Helper T cell differentiation is controlled by the cell cycle. Immunity 9, 229–237 (1998). [PubMed: 9729043]
49. Compagno M, Wang Q, Pighi C, Cheong TC, Meng F-L, Poggio T, Yeap L-S, Karaca E, Blasco RB, Langellotto F, Ambrogio C, Voena C, Wiestner A, Kasar SN, Brown JR, Sun J, Wu CJ, Gostissa M, Alt FW, Chiarle R, Phosphatidylinositol 3-kinase δ blockade increases genomic instability in B cells. Nature 542, 489–493 (2017). [PubMed: 28199309]
50. Zan H, Casali P, Epigenetics of peripheral B-cell differentiation and the antibody response. Front. Immunol 6, 631 (2015). [PubMed: 26697022]
51. Tsagaratou A, Äijö T, Lio C-W, Yue X, Huang Y, Jacobsen SE, Lähdesmäki H, Rao A, Dissecting the dynamic changes of 5-hydroxymethylcytosine in T-cell development and differentiation. Proc. Natl. Acad. Sci. U.S.A 111, E3306–E3315 (2014). [PubMed: 25071199]
52. Oakes CC, Seifert M, Assenov Y, Gu L, Przekopowitz M, Ruppert AS, Wang Q, Imbusch CD, Serva A, Koser SD, Brocks D, Lipka DB, Bogatyrova O, Weichenhan D, Brors B, Rassenti L, Kipps TJ, Mertens D, Zapatka M, Lichter P, Döhner H, Küppers R, Zenz T, Stilgenbauer S, Byrd JC, Plass C, DNA methylation dynamics during B cell maturation underlie a continuum of disease phenotypes in chronic lymphocytic leukemia. Nat. Genet 48, 253–264 (2016). [PubMed: 26780610]
53. Lee CH, Melchers M, Wang H, Torrey TA, Slota R, Qi C-F, Kim JY, Lugar P, Kong HJ, Farrington L, van der Zouwen B, Zhou JX, Lougaris V, Lipsky PE, Grammer AC, Morse HC III, Regulation of the germinal center gene program by interferon (IFN) regulatory factor 8/IFN consensus sequence-binding protein. J. Exp. Med 203, 63–72 (2006). [PubMed: 16380510]
54. Ko M, An J, Pastor WA, Koralov SB, Rajewsky K, Rao A, TET proteins and 5-methylcytosine oxidation in hematological cancers. Immunol. Rev 263, 6–21 (2015). [PubMed: 25510268]
55. Ko M, Bandukwala HS, An J, Lamperti ED, Thompson EC, Hastie R, Tsangaratou A, Rajewsky K, Koralov SB, Rao A, Ten-Eleven-Translocation 2 (TET2) negatively regulates homeostasis and differentiation of hematopoietic stem cells in mice. Proc. Natl. Acad. Sci. U.S.A 108, 14566–14571 (2011). [PubMed: 21873190]
56. Jabara HH, Chaudhuri J, Dutt S, Dedeoglu F, Weng Y, Murphy MM, Franco S, Alt FW, Manis J, Geha RS, B-cell receptor cross-linking delays activation-induced cytidine deaminase induction and inhibits class-switch recombination to IgE. J. Allergy Clin. Immunol 121, 191–196.e2 (2008). [PubMed: 17900678]
57. Lentini A, Lagerwall C, Vikingsson S, Mjoseng HK, Douvlataniotis K, Vogt H, Green H, Meehan RR, Benson M, Nestor CE, A reassessment of DNA-immunoprecipitation-based genomic profiling. Nat. Methods 15, 499–504 (2018). [PubMed: 29941872]
58. Picelli S, Faridani OR, Björklund ÅK, Winberg G, Sagasser S, Sandberg R, Full-length RNA-seq from single cells using Smart-seq2. Nat. Protoc 9, 171–181 (2014). [PubMed: 24385147]
59. Ramírez F, Ryan DP, Grüning B, Bhardwaj V, Kilpert F, Richter AS, Heyne S, Dündar F, Manke T, deepTools2: A next generation web server for deep-sequencing data analysis. Nucleic Acids Res 44, W160–W165 (2016). [PubMed: 27079975]
60. Xi Y, Li W, BSMAP: Whole genome bisulfite sequence MAPping program. BMC Bioinformatics 10, 232 (2009). [PubMed: 19635165]
61. Heinz S, Benner C, Spann N, Bertolino E, Lin YC, Laslo P, Cheng JX, Murre C, Singh H, Glass CK, Simple combinations of lineage-determining transcription factors prime cis-regulatory elements required for macrophage and B cell identities. Mol. Cell 38, 576–589 (2010). [PubMed: 20513432]
62. Robinson MD, McCarthy DJ, Smyth GK, edgeR: A Bioconductor package for differential expression analysis of digital gene expression data. Bioinformatics 26, 139–140 (2010). [PubMed: 19910308]
63. The ENCODE Project Consortium, An integrated encyclopedia of DNA elements in the human genome. Nature 489, 57–74 (2012). [PubMed: 22955616]

64. Buenrostro JD, Giresi PG, Zaba LC, Chang HY, Greenleaf WJ, Transposition of native chromatin for fast and sensitive epigenomic profiling of open chromatin, DNA-binding proteins and nucleosome position. Nat. Methods 10, 1213–1218 (2013). [PubMed: 24097267]

65. Chavez L, Jozefczuk J, Grimm C, Dietrich J, Timmermann B, Lehrach H, Herwig R, Adjaye J, Computational analysis of genome-wide DNA methylation during the differentiation of human embryonic stem cells along the endodermal lineage. Genome Res 20, 1441–1450 (2010). [PubMed: 20802089]

66. Äijö T, Yue X, Rao A, Lähdesmäki H, LuxGLM: A probabilistic covariate model for quantification of DNA methylation modifications with complex experimental designs. Bioinformatics 32, i511–i519 (2016). [PubMed: 27587669]

67. Lin X, Sun D, Rodriguez B, Zhao Q, Sun H, Zhang Y, Li W, BSeQC: Quality control of bisulfite sequencing experiments. Bioinformatics 29, 3227–3229 (2013). [PubMed: 24064417]

68. Song Q, Decato B, Hong EE, Zhou M, Fang F, Qu J, Garvin T, Kessler M, Zhou J, Smith AD, A reference methylome database and analysis pipeline to facilitate integrative and comparative epigenomics. PLOS ONE 8, e81148 (2013). [PubMed: 24324667]

69. Kim D, Langmead B, Salzberg SL, HISAT: A fast spliced aligner with low memory requirements. Nat. Methods 12, 357–360 (2015). [PubMed: 25751142]

70. Kim D, Pertea G, Trapnell C, Pimentel H, Kelley R, Salzberg SL, TopHat2: Accurate alignment of transcriptomes in the presence of insertions, deletions and gene fusions. Genome Biol 14, R36 (2013). [PubMed: 23618408]

71. Anders S, Pyl PT, Huber W, HTSeq—A Python framework to work with high-throughput sequencing data. Bioinformatics 31, 166–169 (2015). [PubMed: 25260700]

72. Leek JT, svaseq: Removing batch effects and other unwanted noise from sequencing data. Nucleic Acids Res 42, e161 (2014).

73. Wu M, Gu L, TCseq: Time course sequencing data analysis. R package version 1.4.0, (2018).

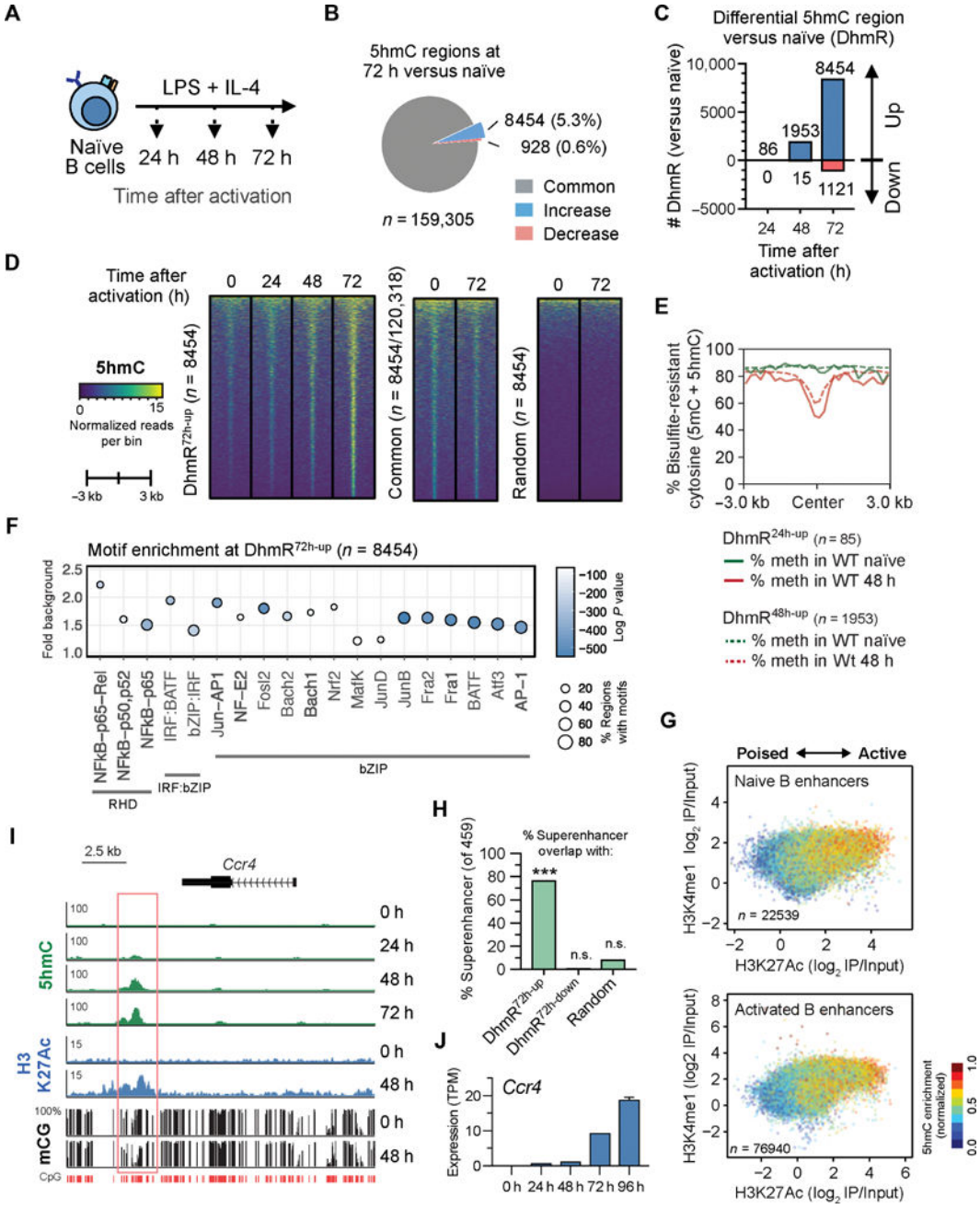

Fig. 1. Dynamic changes in 5hmC during B cell activation.

(**A**) Flowchart of experiments. (**B**) Comparison between 5hmC-enriched regions in unstimulated and activated B cells (72 hours). One hundred ninety-three regions represented only in naïve B cells were not shown. (**C**) Number of DhmRs. (**D**) Kinetics of 5hmC modification in the DhmR$^{72h\text{-}up}$ (left). There is no increase in the same number of randomly chosen common 5hmC-marked regions (middle) and random regions (right). 5hmC enrichment is shown as normalized reads per 100-bp bin. (**E**) The 85 and 1953 regions with increased 5hmC in 24-hour- and 48-hour-activated B cells relative to naïve B cells show decreased “methylation” (bisulfite-resistant cytosine, 5mC + 5hmC) at their centers 48 hours

after activation. Average methylation was calculated for each 200-bp bin across 6 kb. (**F**) Motif enrichment analysis of $DhmR^{72h\text{-}up}$. Common 5hmC-enriched regions were used as background for analysis. The *y* axis indicates the fold enrichment versus background, circle size indicates the percentage of regions containing the respective motif, and the color indicates the significance ($\log_{10}$ *P* value). (**G**) 5hmC is enriched at active ($H3K4me1^{+}$ $H3K27Ac^{hi}$) relative to poised ($H3K4me1^{+}$ $H3K27Ac^{lo}$) enhancers in both activated and naïve B cells. The *y* and *x* axes indicate the levels ($\log_2$) of H3K4me1 and H3K27Ac relative to input, respectively. (**H**) A substantial fraction of superenhancers (352 of 459, 76.7%) identified by high H3K27Ac enrichment overlap with $DhmR^{72h\text{-}up}$. Fisher's exact test was used to analyze the significance. $^{***}P < 0.01$ ($P = 8.9 \times 10^{-266}$). n.s., not significant. (**I**) *Ccr4* locus (mm10; chr9:114,484,000 to 114,501,000) as an example of a region with increased 5hmC, increased H3K27Ac, and decreased CpG methylation after activation. The red track indicates CpGs that were included for analysis based on coverage. (**J**) Kinetics *Ccr4* mRNA expression (by RNA-seq) in activated B cells. See also fig. S1.

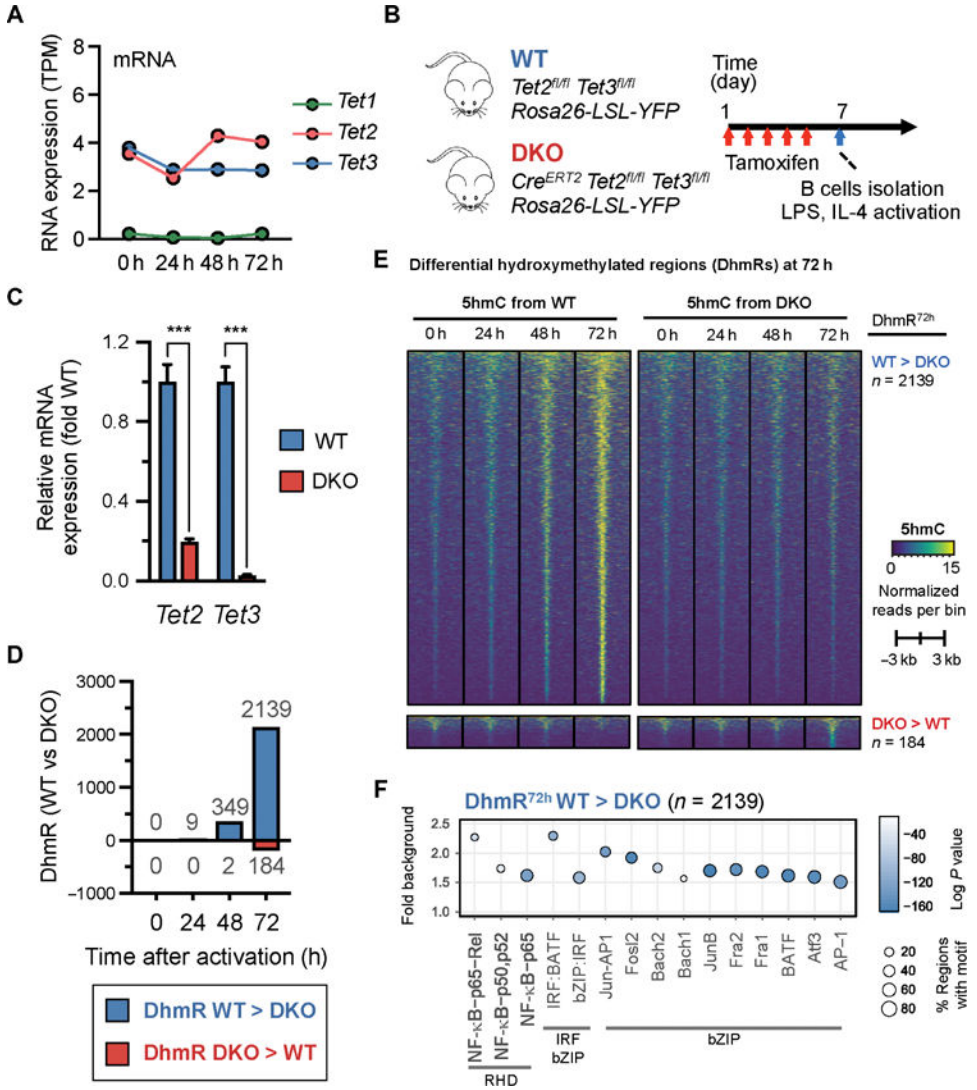

Fig. 2. Comparison of 5hmC modification in WT and *Tet2/3* DKO B cells.

(**A**) Mean mRNA expression for TET family members (from RNA-seq). TPM, transcripts per million. (**B**) Description of mice and flowchart of experiment. (**C**) *Tet2* and *Tet3* are efficiently deleted. *Tet2* and *Tet3* expression in B cells from tamoxifen-treated WT control and *Tet2/3* DKO mice [as described in (B)] were analyzed by qRT-PCR. Data were normalized to *Gapdh* within sample and subsequently to the value from WT. A representative experiment is shown (two independent experiments with three technical replicates). ****P* < 0.01. (**D**) Number of differential 5hmC-enriched regions (DhmR) between WT and *Tet2/3* DKO B cells. (**E**) Kinetics of 5hmC enrichment from WT (left) and *Tet2/3* DKO (right) at DhmRs^{72h} between WT and DKO [72 hours, (D)]. Regions with decreased 5hmC in DKO are shown above (WT > DKO) and those with increased 5hmC are shown below (DKO > WT). 5hmC enrichment is shown in normalized reads per 100-bp bin. (**F**) Motif enrichment analysis of DhmR$^{72h\text{-WT > DKO}}$ (analyzed as in Fig. 1F). See also fig. S2.

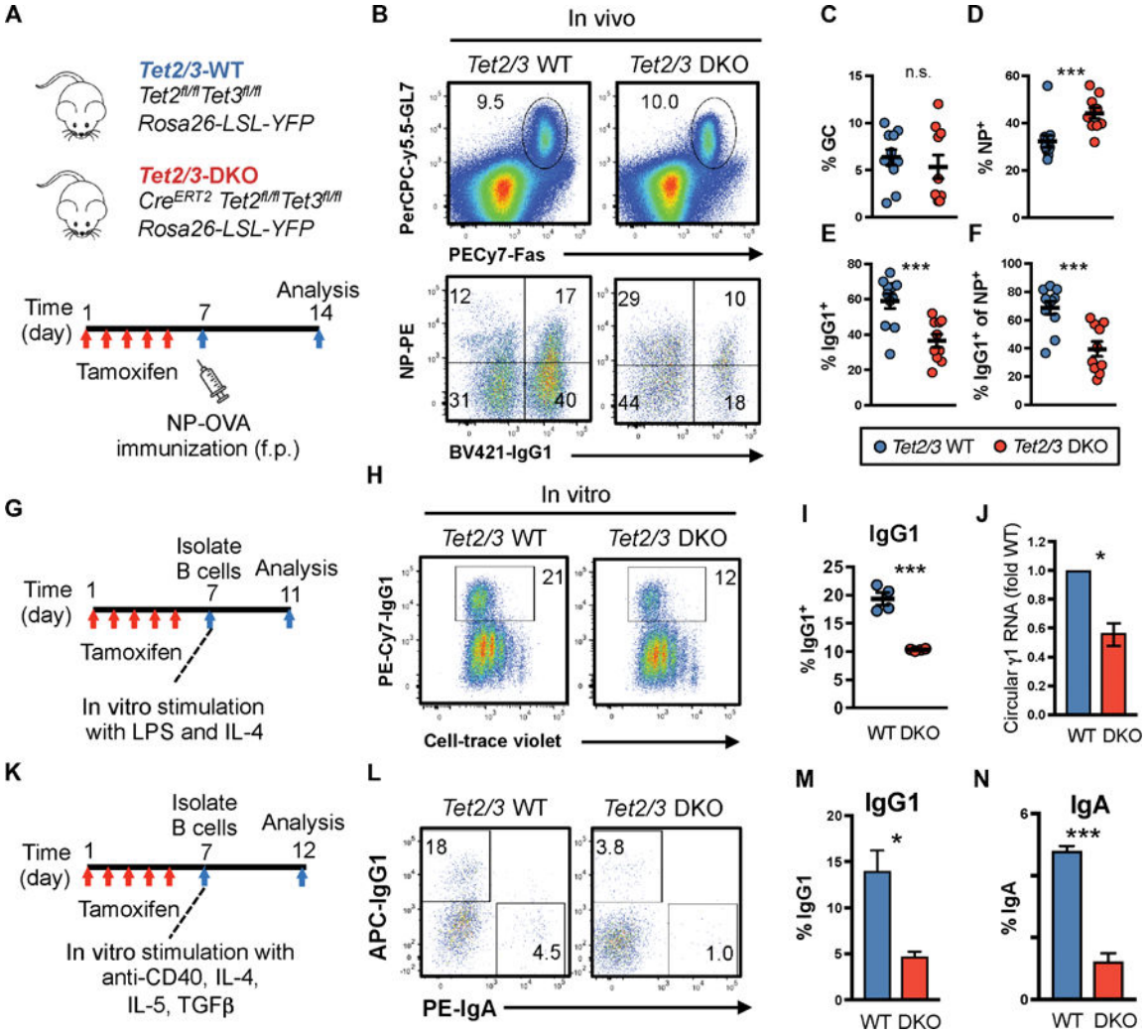

Fig. 3. TET proteins facilitate CSR.

(**A**) Flowchart of in vivo experiment. f.p., footpad. (**B**) Top: Flow cytometric analysis of $CD19^{+}GL7^{+}Fas^{+}$ GC B cells at the draining popliteal lymph nodes from WT and *Tet2/3* DKO mice after NP-OVA immunization as in (A). Bottom: Decreased IgG1-switched cells among GC B cells in *Tet2/3* DKO (YFP^{+} GC B–gated) compared with WT mice (GC B–gated). (**C** to **F**) Quantification of experiments shown in (B). Data shown are aggregated results from two independent experiments. Means and SEs are shown. WT, $n = 11$; DKO, $n = 12$. (**G**) Flowchart of in vitro IgG1 switching. Cells were labeled with Cell trace violet and activated for 4 days with LPS and IL-4. (**H** and **I**) Flow cytometry plots (H) and quantification (I) of IgG1-switched B cells in *Tet2/3* DKO ($n = 4$) and WT ($n = 4$) mice. Representative of at least three independent experiments. (**J**) Circular γ1 transcript was quantified by qRT-PCR and normalized to *Gapdh* and then to the level of WT. Representative experiment of two independent experiments with three technical replicates. (**K**) Flowchart of in vitro IgA switching. Cells were activated for 5 days with anti-CD40, rmIL-4, rmIL-5, and rhTGFβ. (**L** to **N**) Flow cytometry plots (L) and quantification (M and N) of IgG1-switched (M) and IgA-switched cells (N). Representative of three independent

experiments with three technical replicates. Statistical significance was calculated using unpaired two-tailed *t* test. $*P < 0.05$, $***P < 0.01$. See also fig. S3.

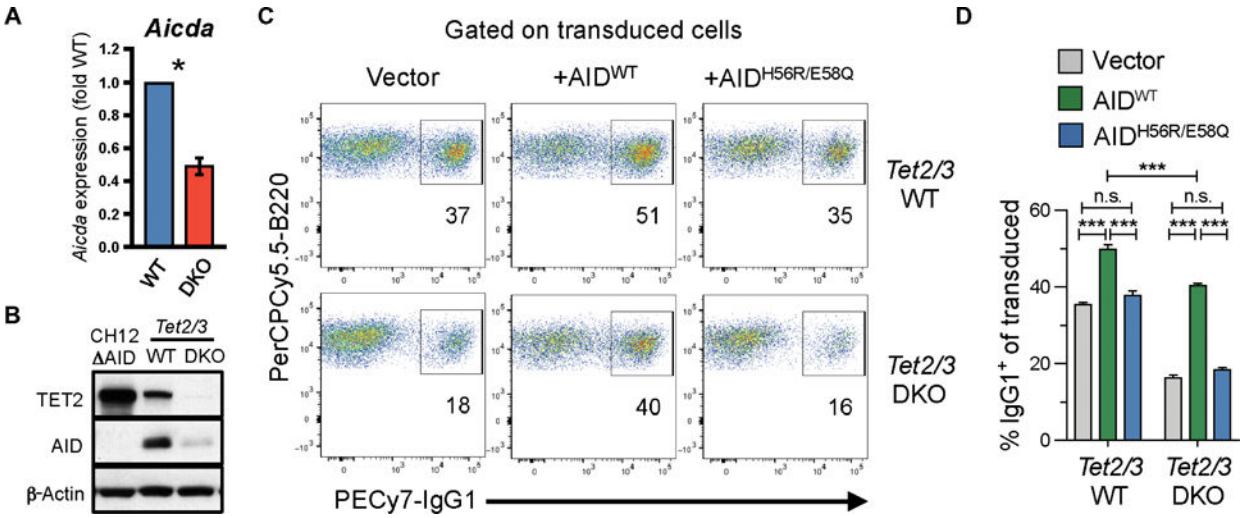

Fig. 4. TET2/3 facilitate CSR by regulating expression of the cytidine deaminase AID.

(**A**) qRT-PCR analysis of *Aicda* mRNA expression in WT and *Tet2/3* DKO B cells activated 4 days with LPS and IL-4. *Aicda* expression was normalized to *Gapdh* and then to the level in WT. Data shown are representative of two independent experiments with three technical replicates. $*P < 0.05$. (**B**) Immunoblotting of whole-cell lysates from day 4 activated WT and *Tet2/3* DKO with indicated antibodies. Left lane contains lysate from the AID-KO CH12 B cells as a control for the specificity of anti-AID antibody. β-Actin was used as loading control. Data shown are representative of two independent experiments. See also fig. S4D. (**C** and **D**) WT and *Tet2/3* DKO B cells were transduced with empty vector (Thy1.1, left), WT AID (AID^{WT}, middle), or catalytically inactive AID ($AID^{H56R/E58Q}$, right). Gated on live-transduced B cells ($CD19^+$ $Thy1.1^+$). Representative flow cytometry plots (C) and quantification (D) are shown. Data shown are representative of three independent experiments. $***P < 0.01$. See also fig. S4.

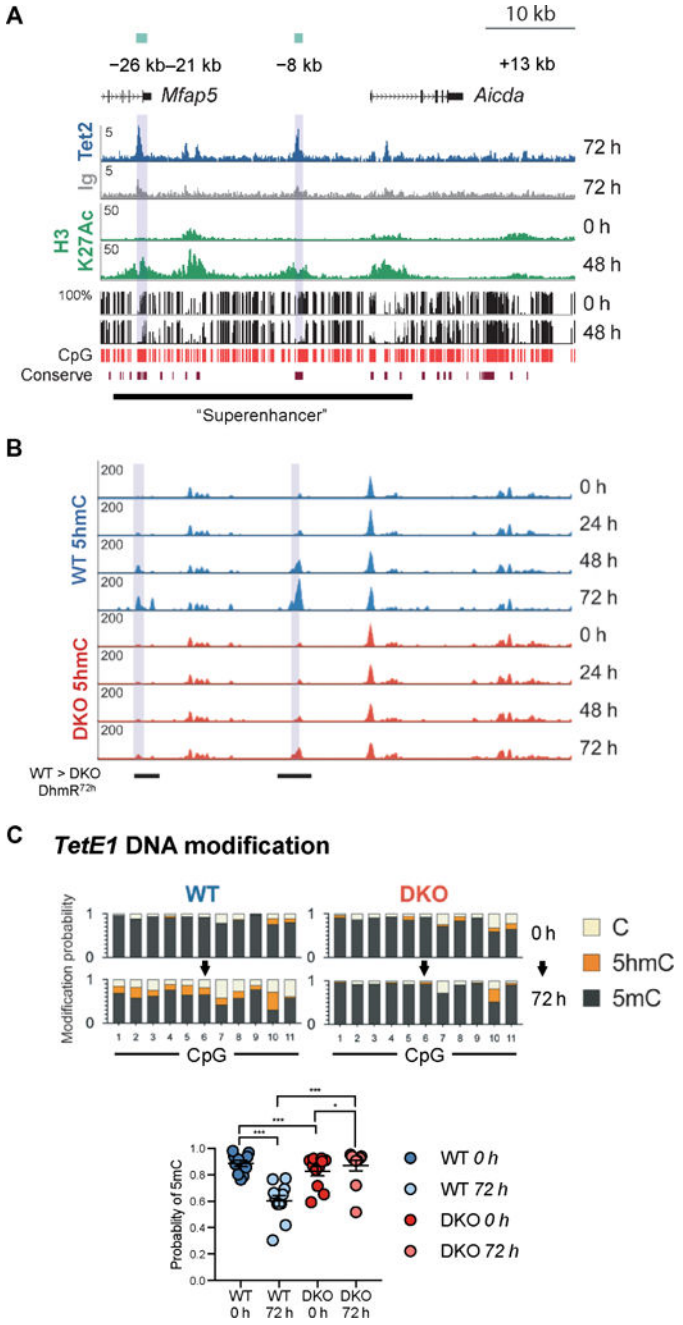

Fig. 5. TET2 and TET3 control *Aicda* expression via TET-responsive elements *TetE1* and *TetE2*.

Diagram shows two conserved TET-responsive elements *TetE1* and *TetE2* located 5′ of the *Aicda* gene (labeled with green rectangles and gray shades). (**A**) Top two tracks: ChIP-seq analysis showed that TET2 (blue track) specifically bound to multiple elements in the *Aicda* locus (mm10; chr6:122,523,500 to 122,576,500) after activation when compared with Ig control (gray track). Middle track (green): Increased H3K27Ac after activation. Bottom track: Activation induced DNA demethylation at *TetE1* and *TetE2*. WGBS showing DNA methylation (5mC + 5hmC) in naïve and 48-hour-activated B cells (mCG; black track). CpGs included in the analysis are indicated by red lines (red track). Bottom track indicates

the conserved DNA elements among placental animals ("Conserve"). A previously identified superenhancer is indicated. For TET2 and Ig, scales indicate per 10 million reads; H3K27Ac, quantile-normalized reads; BS, percentage of bisulfite-resistant cytosine. (**B**) Activation induced TET2/3-dependent 5hmC deposition at *Aicda* distal elements. 5hmC modification was analyzed in WT and *Tet2/3* DKO B cells activated as in Fig. 3G. Differentially 5hmC-enriched regions between WT and DKO after 72 hours activation are shown (WT > DKO $DhmR^{72h}$). Scales indicate quantile-normalized reads. (**C**) TET2/3 deposit 5hmC and demethylate *TetE1*. Top: CpG modifications (5hmC, 5mC, and C) at *TetE1* were analyzed by oxBS-seq using DNA isolated from WT and *Tet2/3* DKO B cells before (0 hours) and after (72 hours) activation. Bottom: Quantification of the probability of 5mC modification on all CpGs in *TetE1*. The difference between samples was compared by using the Wilcoxon rank-sum test. $*P < 0.05$, $***P < 0.01$. See also fig. S5H.

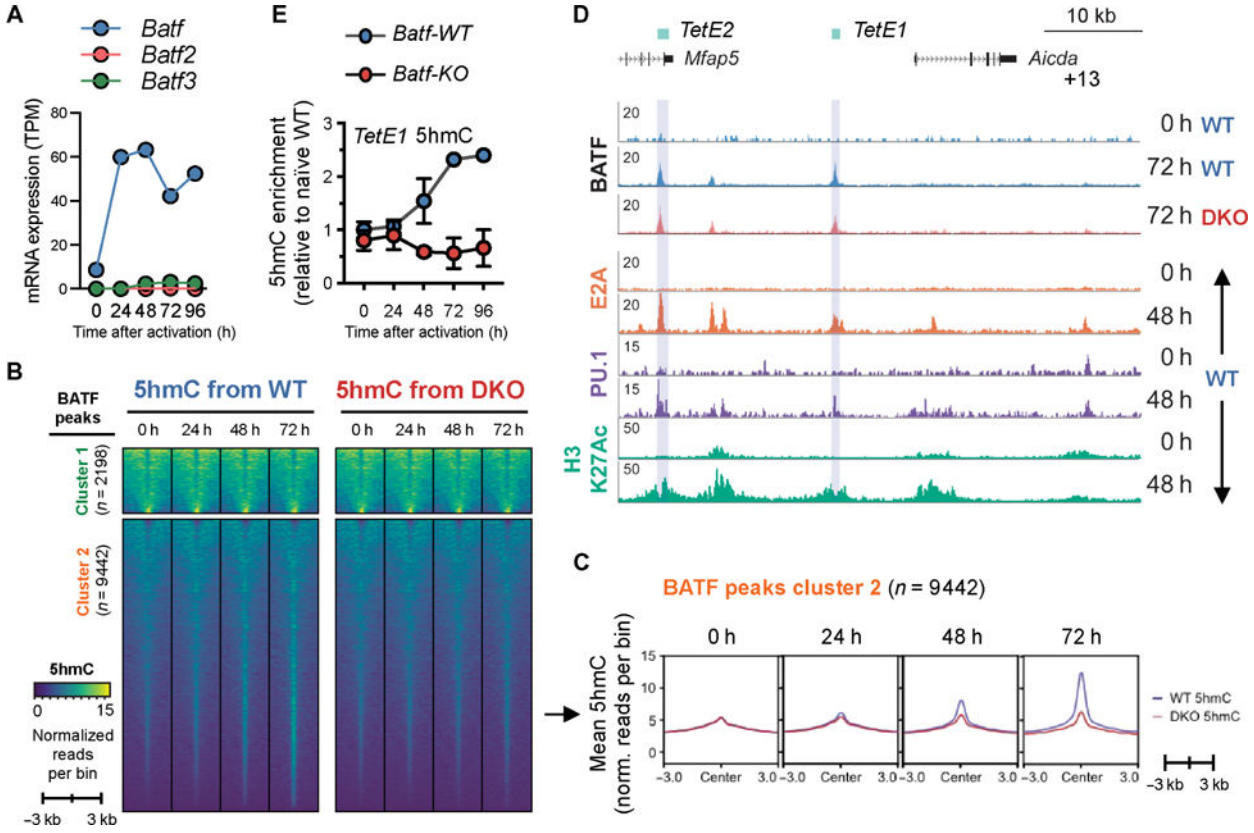

Fig. 6. BATF facilitates TET protein–mediated hydroxymethylation at *TetE1*.

(**A**) Mean mRNA expression (RNA-seq) of *Batf* family (*Batf1 to Batf3*). (**B** and **C**) BATF binding correlates with 5hmC enrichment. WT BATF peaks were divided into two clusters on the basis of the pattern of 5hmC distribution. (B) Cluster 1 showed a broad 5hmC distribution, with the 5hmC level remaining unchanged after activation and in the absence of TET2/3 (top, compare "5hmC from WT" with "5hmC from DKO"). In contrast, a substantial proportion of regions in cluster 2 showed progressive TET-dependent 5hmC modification after activation (bottom), as further illustrated in (C) as line plots. Data shown are mean enrichment per 100-bp bin. (**D**) Recruitment of BATF and other transcription factors to *Aicda* enhancers. Top three tracks: Genome browser view of BATF-binding in unstimulated and 72-hour-activated WT (blue) and *Tet2/3* DKO B cells (red) at the *Aicda* locus. Note that loss of *Tet2/3* has no significant effect on BATF recruitment (compare WT and DKO, tracks 2 and 3; see also fig. S8G). Activation also induced E2A and PU.1 binding to *Aicda* enhancers (orange and purple tracks). Green tracks indicate H3K27Ac. Coordinates are chr6:122,523,500 to 122,576,500 (mm10). See also fig. S8. (**E**) BATF is required for 5hmC modification at *TetE1*. *Batf-WT* and *Batf-KO* B cells were activated with LPS and IL-4 for 4 days. 5hmC modification at *TetE1* was quantified using AbaSI-qPCR.